Molecular Characterization of *spa, hld, fmhA*, and l*ukD* Genes and Computational Modeling the Multidrug Resistance of *Staphylococcus* Species through *Callindra harrisii* Silver Nanoparticles

Muhammad Waseem, Muhammad Naveed,* Shafiq ur Rehman, Syeda Izma Makhdoom, Tariq Aziz,* Metab Alharbi, Abdulrahman Alsahammari, and Abdullah F. Alasmari

ACCESS | Metrics & More | Article Recommendations

ABSTRACT: The problem of multidrug resistance in bacterial pathogens is significant and is related to the high morbidity and death rates of living things due to increased levels of beta-lactamases. Plant-derived nanoparticles have gained a great significance in the field of science and technology to combat bacterial diseases, especially multidrug-resistant bacteria. This study examines the multidrug resistance and virulent genes of identified pathogenic *Staphylococcus* species obtained from Molecular Biotechnology and Bioinformatics Laboratory (MBBL), culture collection. The polymerase chain reaction-based characterization of *Staphylococcus aureus* and *Staphylococcus argenteus* having ON875315.1 and ON876003.1 accession IDs revealed the presence of the *spa, LukD, fmhA*, and *hld* genes. The green synthesis of silver nanoparticles (AgNPs) was carried out by utilizing the leaf extract of *Calliandra harrisii*, of which metabolites act as capping and reducing agents for the precursor of nano-synthesis, i.e., AgNO$_3$ of 0.25 M. The synthesized AgNPs were characterized via UV−vis spectroscopy, Fourier transform infrared spectroscopy, scanning electron microscopy, and energy-dispersive X-ray analysis which inferred the bead-like shape of our nanoparticles with the size of 2.21 nm with the existence of aromatic and hydroxyl functional groups at surface plasmon resonance of 477 nm. The antimicrobial activity by AgNPs showed 20 mm inhibition of *Staphylococcus* species as compared to the vancomycin and cefoxitin antibiotics along with crude plant extract, which showed a minimum zone of inhibition. The synthesized AgNPs were also analyzed for various biological activities like anti-inflammatory with 99.15% inhibition in protein denaturation, antioxidant with 99.8% inhibition in free radical scavenging, antidiabetic with 90.56% inhibition of alpha amylase assay, and anti-haemolytic with 89.9% inhibition in cell lysis which shows good bioavailability and biocompatibility of the nanoparticles with the biological system of the living being. The amplified genes (*spa, LukD, fmhA*, and *hld*) were also analyzed for their interaction with AgNPs computationally at the molecular level. The 3-D structure of AgNP and amplified genes was retrieved from ChemSpider (ID: 22394) and Phyre2 online server, respectively. The binding affinities of AgNP with *spa, LukD*, fmhA, and hld were −7.16, −6.5, −6.45, and −3.3 kJ/mol, respectively, which infers a good docking score except of *hld* which is −3.3 kJ/mol due to its small size. The salient features of biosynthesized AgNPs proved to be an effective approach in combating the multidrug-resistant *Staphylococcus* species in the future.
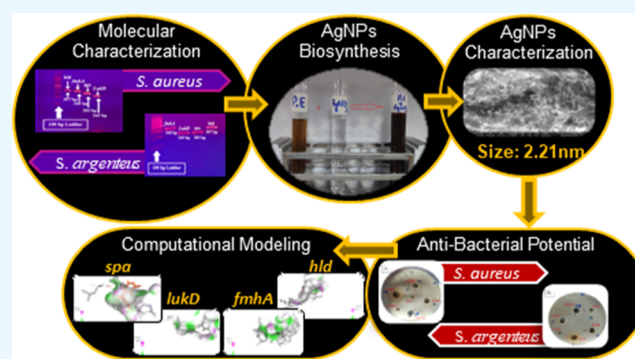
1. INTRODUCTION

Multidrug-resistant organisms are bacteria that can no longer be controlled or killed by some antibiotics because they have developed a resistance to those antibiotics. As a result of the widespread use of antibiotics in human medicine, farm animals and fish raised for food have developed antibiotic resistance, which has led to the selection of pathogenic bacteria.[1] Bacteria may develop multidrug resistance through one of two mechanisms. First, within a single cell, these bacteria may amass several genes, each of which codes for drug resistance.

This build-up typically takes place on resistance (R) plasmids.

Second, the increased expression of genes that create multidrug

Table 1. Sequences of Different Gene Primers

primer name	forward primer	reverse primer	product size	reference
FmhA	CGTTGACTTCGGATGAG	CACCGTCTGCATTGCGTA	345 bp	synthesized
LukD	GCAGCTCAACATATCACAC	ACCGCCCCAATAAAACTGTG	243 bp	synthesized
Spa(Protein A)	GTGGCGTAACACCTGCTG	GAAGCCGTTACGTTGCGC	293 bp	synthesized
Delta Hemolysin	GAATTTGTTCACTGTGTCG	TTTACACCACTCTCCTCAC	357 bp	(Marconi et al., 2005)

efflux pumps, which extrude a variety of medications, may also contribute to multidrug resistance.[2]

Staphylococcus aureus is an opportunistic, emerging, facultative Gram-positive bacteria linked to several nosocomial and community-acquired infections. Additionally, it has been linked to toxic shock syndrome, pneumonia, and severe skin infections. A versatile pathogen, *S. aureus* can infect a wide range of hosts, including sheep, pigs, cattle, and poultry.[3] *S. aureus* has developed resistance and tolerance mechanisms against a variety of antibiotics, from specific to broad-spectrum, including penicillin, quinolone, methicillin, and vancomycin, thanks to its inherent and adaptive characteristics. This bacterium, which is portrayed as multidrug resistant bacteria, encodes a hydro-lyzing enzyme to produce an acquired resistance mechanism against antibiotics (MDR).[4] The multidrug-resistant pathogen Methicillin-resistant *S. aureus* (MRSA) has developed resistance to frequently altered antibiotics. Penicillin-binding proteins were altered by MRSA to carry out its function (PBP2). Peptidoglycan is biosynthesized by bifunctional transglucosy-lase-transpeptidase and normal PBP2 (cell wall).[5] Here, MRSA produces modified genes that code for PBP2a, which inactivates the transpeptidase (TP) of normal PBP2 and prevents -lactams from accessing the serine active site of TP, rendering -lactams resistant. *S. aureus* causes the most commonly infective endocarditis, which is a deadly disease.[6] In this infection, the formation of bacterial colonies in the endothelial exposure elicits the production and deposition of other tissue factors or platelets and causes the vegetation of the bacteria. When these thrombotic growths become colonialized, infective Endocarditis can result in those areas. This bacterium may be evidence of some epithelial infections, and they begin with small lesions to various life-threatening diseases.[7]

Microbial resistance to current antibiotic therapy is a significant contributor to implant failure and subpar clinical outcomes in orthopaedic surgery. Recent developments in complex antimicrobial nanotechnologies provide numerous opportunities to successfully eradicate resistant pathogens and prevent resistance from occurring through unique processes.[8] Due to their programmable physicochemical properties, nano-materials can be made to be bactericidal, antifouling, immunomodulating, and capable of precisely delivering antibacterial chemicals to the infection location. Nanoparticles can combat antibiotic resistance by using a variety of novel bactericidal pathways to produce the desired antimicrobial activity.[9] For instance, the active ingredient in antimicrobials based on silver nanoparticles (AgNPs) is free Ag^+ ions. Silver ions disrupt electron transport across the bacterial membrane and harm DNA. In order to increase their broad-spectrum activity while decreasing their toxicity toward mammalian cells, nanomaterials' surface chemistry is crucial in controlling how they interact with bacteria.[10]

The current study reveals a cost-effective and efficient method to overcome the resistance and virulence of MRSA at a laboratory scale by utilizing nanotechnology and plant phytochemicals. The virulent genes of *Staphylococcus* species,

i.e., *Spa*, *LukD*, *FmhA*, and *hld* were amplified through polymerase chain reaction (PCR) amplification. The biosynthesis of AgNPs from the leaves extract of *Calliandra harrisii* at optimized parameters were mathematically modeled against various physiochemical and tested against multidrug-resistant *Staphylococcus* species. UV−visible spectrophotometry, scanning electron microscopy (SEM), energy-dispersive X-ray analysis (EDX), and Fourier transform infrared (FTIR) spectroscopy are also used to characterize AgNPs' functionality, size, and shape. The side effects on biological systems caused by the synthesized AgNPs' antioxidant, anti-inflammatory, anti-hemolytic, anti-diabetic, and cytotoxicity activities were also examined. Furthermore, the effect of the AgNPs was also analyzed against the virulent genes *Spa*, *LukD*, *FmhA*, and Hemolysin D computationally.

2. MATERIALS AND METHODS

2.1. Sample Collection. The samples of different bacterial strains were collected from Molecular biotechnology and Bioinformatics Laboratory (MBBL). The collection of samples includes *S. aureus* and *Staphylococcus argenteus.* These species were identified, characterized, and submitted on National Centre of Biotechnology Information (NCBI) having ON875315.1 and ON876003.1 accession ID.

2.2. PCR Amplification. PCR machine work with the combination of enzymatic process and thermodynamic techniques and it work on some optimized conditions. Genes *LukD*, *FmhA*, *Spa*, and Delta Hemolysin were amplified with their specific primers.

1. PCR reaction procedure
2. Take autoclaved PCR tubes and add 12.5 μL of master mix into it with the help of a micro pipette.
3. After this, add 2 μL of DNA sample into this PCR tube.
4. Then, added 8.5 μL ampule water into it.
5. Added one by one 1 μL of forward and reverse primers into each tube.
6. Mixed all the tubes well with the help of vortex.
7. Put all these prepared samples in to the PCR machine.
8. Adjust the profile according to your requirement and start the reaction.

2.2.1. Amplification of LukD, FmhA, Spa, and Delta Hemolysin. The virulent and resistant genes (i.e., *LukD*, *FmhA*, *Spa*, and *hld*) were amplified in the different strains of *Staphylococcus*. The amplified genes were visualized on 2% agarose gel, and bands confirmed that these genes are present in the different strains of *Staphylococcus*. When amplification completed, then these samples were run on an agarose gel with a 1 Kb ladder for the conformation of band and gene size (Table 1).

2.3. Preparation of Plant Extract of *C. harrisii*. The leaves of the plant *C. harrisii* for research purposes were collected from the botanical garden of the University of Punjab Lahore. When plant leaves were collected, wash them with distilled water and dry them under shade. The dried leaves of *C. harrisii* were

ground in an electronic grinder. In 1000 mL of a beaker, 500 mL of distilled water and 20 g of *C. harrisii* plant powder were added following the method of Naveed et al..[11,12] The beaker was placed on a hot plate magnetic stirrer for 2 h by adjusting its temperature at 60 °C and 1500 rpm to obtain the plant extract. The solution was filtered after 2 h using Whatman filter paper No 1. into the conical flask. The filtered solution was stored at 4 °C in the lab refrigerator to use further for the synthesis of silver nanoparticles, phytochemical screening, and determination of reducing the power of *C. harrisii*.[13]

2.4. Phytochemical Screening of *C. harrisii* Leaves Extract. *2.4.1. Wagner's Test.* Alkaloids in the plant leaf extract were screened by performing Wagner's test. For this purpose, 2.5−3 mL of plant leaf extract was taken into the test tube. After that, 1 mL of diluted HCl and 0.5−1 mL of Wagner's reagent were added into the test tube with leaves extract. After adding both chemicals, the test tube was shaken vigorously and then observed the color change; if the color converts into reddish brown, it indicates the presence of alkaloids.

2.4.2. Foam Test. Almost all plants have saponins; detecting saponins in the *C. harrisii* leaves extract was examined by performing a foam test. 4−5 mL of plant leaf extract was taken into the test tube. 4−5 mL of distilled water was added into the same test tube with a plant extract and was shaken vigorously; if the foam's stable formation is observed, it indicates the presence of saponins.

2.4.3. Ferric Chloride Test. A Ferric chloride test was performed to screen the phenolic compounds in the *C. harrisii* plant leaves extract. For this test, 4−5 mL of leaves extract was taken into the test tube and 0.5−1 mL of neutral 5% ferric chloride solution was added in the same test tube. Plant extract reacts with ferric chloride solution and produces a blue-green color, indicating the presence of phenolic compounds in the plant extract.

2.4.4. Braymer's Test. Tannins are the compounds that are present in the plants; for the research, tannin compounds were screened in the *C. harrisii* plant leaves extract by performing Braymer's test. This test was performed by adding 1.5−2 mL of distilled water and 0.5−1 mL of ferric chloride solution into the 1.5−2 mL of plant leaves extract of *C. harrisii*. Ferric chloride reacts with the leaves extract and makes a green precipitate, indicating the presence of tannin compounds in the *C. harrisii* plant.

2.4.5. Salkowski's Test. Terpenoids are the phytochemicals compounds present in almost every plant; for the research, Salkowski's test was performed to screen the terpenoids in the *C. harrisii* plant leaves extract. 2 mL of plant leaves extract was taken into the test tube and 2 mL of chloroform and 2 mL of concentrated H_2SO_4 were added into the same test tube with leaves extract and mixed. Chloroform and H_2SO_4 react with the plant leaf extract and produce the yellow color, indicating terpenoids in the *C. harrisii* plant extract.

2.4.6. Bontrager's Test. Quinones are the phytochemical compounds that are immensely present in plants. Quinones are screened out for the research by performing Bontrager's test. 3 mL of plant extract was added to the test tube and the same amount of chloroform was added to the same test tube. When chloroform is added into the plant extract, it makes a separate layer of plant extract and chloroform. 5% potassium hydroxide was added to the layer formed. If the red color occurs in the layer formed between the plant extract and chloroform, it indicates the presence of quinones.

2.4.7. Keller Killian's Test. Cardiac Glycosides phytochemicals of *C. harrisii* were screened out by performing Keller Killian's test. 2 mL of plant extract was taken into the test tube and 2 mL of concentrated HCl, sodium nitroprusside, and NaOH were added. Observed the color change; if it changes from pink to blood red, it indicates the presence of cardiac glycosides.

2.4.8. Glycosides Test. A glycosides test was performed to screen the phytochemical glycosides. 1.5−2 mL of plant leaves extract of *C. harrisii* was mixed with 2.5−3 mL chloroform and 10% ammonia solution into the same test tube. Pink color formation indicates the presence of glycosides in the plant extract.

2.4.9. Alkaline Reagent Test. Flavonoids from the *C. harrisii* plant were screened by performing an alkaline reagent test. To this end, a few drops of sodium hydroxide was added into the 1.5−2 mL of plant leaves extract in the test tube. If yellow color appears, it indicates the presence of flavonoids.

2.4.10. Precipitate Test. The phytochemical phlobatannins were screened by performing a precipitate test. 1 mL of *C. harrisii* plant was taken in the test tube and a few drops of 2% HCl were added into the same test tube; the formation of red color in the test tube indicates the presence of phlobatannins in the extract of *C. harrisii*.

2.5. Characterization of Reducing the Power of *C. harrisii*. The determination of reducing the power of leaves of *C. harrisii* was done by the transition of Fe^{3+}/ferricyanide complex to Fe^{2+}/ferricyanide complex, which means the reduction of AgNPs also occurred.

2.5.1. Standard Solution Preparation. The standard solution was made by 1 M ascorbic acid to check the reduction power of the plant extract at various concentrations of 15, 30, 45, 60, and 75 μg/mL.

2.5.2. Test Sample Preparation. The leaves extract of *C. harrisii* was used to test the samples of the test sample preparation. The standard solutions used for this test are 15, 30, 45, 60, and 75 μg/mL.

2.5.3. Method for Determination of Reducing Power. The standard mentioned above and the test solution were mixed with the phosphate buffer with a 2.5 mL concentration and the 1% potassium ferricyanide $[K_3Fe\,(C.N)_6]$. This method was proceeded by the mixture incubation in the water at 60 degrees Celsius for about 30 min. TCA (trichloroacetic acid) was added when the mixture was cooled. Then, there is centrifugation of the mixed solution at 3000 rpm for about 10 min. There is the assertion of the upper layer after centrifugation with 2.5 mL of distilled water and 0.5 mL freshly prepared ferric chloride solution (0.1%). The absorbance of the prepared solution was measured at 700 nm by a UV−vis spectrophotometer. As a blank, distilled water was used for the analysis. The increase in absorbance 700 nm indicated that the plant extract has the highest reducing power.[14]

2.6. Precursor Preparation of AgNO₃ for Silver NPs. The precursor was prepared for the formation of AgNPs by mixing the $AgNO_3$ in distilled water. First, the stock solution of 1 M of AgNPs was formed in the most suitable conditions in the dark site. When the solution was prepared, the reagent bottle was then covered with an aluminum foil so that the light could not penetrate the solution of the precursor. Then, the working solution of 25 mM was prepared for the formation or synthesis of AgNPs.

2.7. Biological Synthesis of Ag-Nanoparticles. AgNPs were biologically synthesized by adding 25 mM of AgNP

precursor with the leaves extract of *C. harrisii* in the ratio of 1:9. The leaves extract was mixed with a AgNP precursor solution in a dropwise manner. This was continuously stirred in a chamber closed with aluminum foil on the magnetic stirrer at 1500 rpm. This was conducted to avoid light reactions. When there was complete addition of leaves extract, the incubated solution was further centrifuged at 4000 rpm for about 30 min. The pellet was further washed with distilled water about three times. The pellet was dried and poured into an evaporating dish which was further dried in the hot air oven at 80 degrees Celsius for 6−7 h. This pellet was stored in the Eppendorf tube at room temperature.

2.8. Characterization of AgNPs. *2.8.1. Spectrometric Analysis by Spectrophotometer.* Spectrophotometric analysis was performed for the confirmation of the presence of AgNPs. SPR (surface plasmon resonance) analysis was performed to check the band between 200 and 800 nm. This band is associated with the absorption of AgNPs in the area of 250−480 nm, which was activated by the surface plasmon vibration, further identifying the presence of AgNPs.

2.8.2. SEM Analysis. SEM analysis was performed to check the structure of synthesized nanoparticles. Synthesized nanoparticles were dried at room temperature and placed on a double conductive tape. The samples were coated with a platinum-gold coating to increase the synthesized nanoparticles' conductivity. Then, the samples were seen at 12.50 kV voltages.

2.8.3. FTIR Spectroscopy. The functional groups determine the synthesis of AgNPs. FTIR is a technique used to determine the functional groups, and the spectrum was recorded using FTIR. For the FTIR measurements, the solution of AgNPs was centrifuged for 30 min at 1000 rpm.

2.8.4. Energy-Dispersive X-Ray Spectroscopy. AgNPs were analyzed using EDX to identify the components on their surface. For this purpose, certain X-rays are bombarded onto the sample. The recorded diffracted rays are measured to examine the elemental composition, and the findings are displayed on the screen.

2.9. Antimicrobial Activity. For antimicrobial activity, first prepared Luria−Bertani (LB) agar media into the 250 mL flask and autoclaved all equipment and media at 120 °C for 15 min. The disc diffusion method was used to perform the antibacterial activity of different strains of *Staphylococcus*. The nutrient broth is prepared and autoclaved for fresh bacterial strains. After this, 5 mL of nutrient broth was poured into each falcon tube and three falcon tubes were prepared and one colony was picked onto each plate of a different strain of *Staphylococcus* and dissolved it into the falcon tubes and incubated it in the incubator shaker for 24 h and 37 °C. The next day, culture plates were set up by adding sterile LB agar media. Media were formed according to requirements. About 25 mL of the medium was added into germ-free Petri-plates and left at room temperature for 1 day to ensure contamination-free plates. 200 μL of overnight grown cultures of each strain were spread to the LB agar plates and placed an antibiotic disc (vancomycin, fox), 500 μL of AgNP 25 Mm, 500 μL of AgNP 0.1 Mm, 500 μL of AgNP 1 M, and 500 μL of plant extract placed on to the Petri dish and incubated it into the incubator overnight. On the next day the inhibition zone around the disc was calculated and compared to the positive control. A zone of inhibition surrounding the disc confirms the antibacterial properties of the relevant solution. If the zone of inhibition is equal to 12 mm, it will be significant.

2.10. Anti-Inflammatory Analysis. The protein denaturation method studied the anti-inflammatory activity of *C. harrisii* leaves extract and greenly synthesized AgNPs. 1.5−2 mL extract

of *C. harrisii* leaves and biologically synthesized AgNPs with various concentrations of 100, 200, 300, 400, and 500 μg/mL were combined with a 2.8 mL phosphate buffer saline (PBS) solution of pH (6.4) and 0.2 mL of fresh egg white. It was incubated into the water bath for 20 min at room temperature (37 °C). After this incubation, It was put into the water bath for 5 min at 70 °C temperature. To this end, when it is cooled, then the turbidity was measured by a UV−vis spectrophotometer at 660 nm. For this, aspirin drug was used as a control with the same concentration mentioned above for the sample (100, 200, 300, 400, and 500 μg/mL). Then, the anti-inflammatory analysis was performed in the triplicate manner, and protein inhibition was calculated using the below-mentioned formula.

$$\% \text{ inhibition of protein denaturation} = 1 - A_t / A_c \times 100$$

where A_t = absorbance of the test sample and A_c = Absorbance of control.

2.11. Antioxidant Analysis. Screening for antioxidant activity in plant extracts is commonly done using the DPPH (2,2-diphenyl-1-picrylhydrazyl) free radical scavenging method. Leaves extracted of *C. harrisii* and synthesized AgNPs have free radical scavenging and were analyzed using the DPPH-based assay. For this, samples of leaves extract and AgNPs were prepared at different concentrations of 200, 400, 600, 800, and 1000 μL for DPPH analysis. First, 0.1 mM DPPH was prepared and 3.94 mg of DPPH was taken and mixed it into 100 mL of methanol; all this was performed in a dark environment and avoided light contact because when DPPH is in contact with the light, it degrades; when it is prepared, the reagent bottle was wrapped with aluminum foil and kept it in the dark at 30 °C. Test tubes of plant leaf extract and AgNPs with different concentrations mentioned above were prepared and added 0.1 mL of 0.1 nm DPPH in each test tube; incubated all these test tubes into the water bath for 30 min, and after this, the absorbance was measured at 517 nm against the DPPH which was used as the positive control. The free radical analysis was performed in triplicate, and we calculated the percentage for DPPH inhibition using the formula below.

$$\% \text{ DPPH inhibition} = A_0 - A_s / A_0 \times 100$$

where A_0 = absorbance of the control and A_s = absorbance of the test sample.

2.12. Peptide Hemolytic Activity. This activity was performed to determine cytotoxic effects of the samples on the cells. 3 mL of human blood sample was collected, dispensed in a lithium heparin tube, and there was mixing with inversion. Sample was dispensed off in the 15 mL tube and then centrifugation occurs for about 5 min at a rate of 850 × g. The washing of pellet was done three times with PBS at about 4 °C, and the supernatant was discarded when the cells were washed; then, there is the formation of suspension with the chilled PBS by making up the total volume to 20 mL in a falcon tube. The concentration of suspension of blood cell was 180 μL and 2 μL with various concentrations such as Crude 600 μg/mL, 500 μg/ mL which is 50% and 400 μg/mL which is 70%. This suspension was added in the 2 mL tube. This sample was then incubated in the shaking incubator at 80 rev per minute for about 30 min. This sample was then placed on ice for about 5 min after incubation. This was further centrifuged at 1310 rpm. 100 μg of supernatant was aliquoted just after the centrifugation. This was diluted with 900 μL of PBS which was placed on ice for some mins. The absorbance was measured at 630 nm on a Biotek

ELISA plate reader. The positive control was 10% Triton X 100 (100%) and the negative control was PBS (3.97%).

The hemolysis percentage was calculated by utilizing this formula

$$\% \text{ hemolysis} = (\text{Abs. of sample} - \text{Abs. of negative}$$
$$\text{control}) / \text{The abs. of positive control} \times 100$$

2.13. Antidiabetic Activity. The antidiabetic activity was determined using the alpha-amylase test.[15] The different concentrations (200, 400, 600, 800, and 1000 μL) of plant leaves extract and AgNPs prepared in distilled water was used. Alpha-amylase solution was prepared in another falcon tube for this activity; metformin solution was used as a control for this antidiabetic activity. Different concentrations of control, plant extract, and AgNPs (200, 400, 600, 800, and 1000) were added into different test tubes. In each test tube, 10 μL of an alpha-amylase solution was added, mixed, and incubated at 30 °C for 10 min. After the incubation for 10 min, 50 μL of prepared 1% starch solution was added and incubated again for 1 h at 37 °C. At last, 50 μL of 1% iodine solution was added into each test tube and incubated for 30 min at 37 °C, and at the end, absorbance was checked using an Elisa reader at 630 nm.

Antidiabetic percentage was calculated by utilizing this formula

$$\% \text{ inhibition} = [(\text{Abs}_{\text{control}} - \text{Abs}_{\text{sample}}) / \text{Abs}_{\text{sample}}] \times 100$$

2.14. Cytotoxicity Analysis. The percentage cytotoxicity of AgNPs was evaluated by dose-dependent MTT analysis. Exponentially growing cells were counted and 10 000 cells per well were plated, in triplicates, in flat-bottomed 96-well plates (Nunc, Roskilde, Denmark) for both cell lines respectively. The volume of the cells was kept at 100μL per well. Compounds were dissolved in 0.1% DMSO, separately, to obtain different concentrations, i.e., 800, 600, 400, 200, 100, and 50 μg/mL. Each concentration of compounds was added to the 96-well plate to obtain a final volume of ~200 μL/well. In addition, each concentration was tested in triplicate on U87 and HEK 293 cells. Control wells contained solvent control (without drug), standard anticancer drug (doxorubicin), and blank media (without cells). Subsequently, 5 mg of MTT dye (3-[4, 5-dimethylthiazol-2-yl]-2, 5-diphenyltetrazolium bromide) (Invitrogen, Catalogue no #M6494) was dissolved in 1 mL of PBS. Accordingly, 15 μL of prepared MTT solution was added to each well and incubated for 3 h at 37 °C, so that intracellular purple formazan crystals became visible under the microscope. Following the formation of formazan crystals, all the solution from each well was removed. Then, the solubilizing solution, i.e., 150 μL of DMSO, was added to each well. The plates were left at room temperature for a few minutes, while DMSO solution was mixed thoroughly by pipetting up and down to dissolve the formazan crystals. Finally, the absorbance of the cells was measured by a spectrophotometer at 550 nm. The percentage cell viability was calculated using below given formula.

$$\text{cell viability} = (\text{treated cells} - \text{blank}) / (\text{solvent} - \text{blank})$$
$$\times 100 \ \%$$

2.15. Physiochemical Properties. A mathematical equation was used to calculate the density, specific heat, and thermal conductivity of AgNPs and nanoparticle mixtures in the range of 15−45 °C. Additionally, data were collected at the same

temperature ranges by combining AgNPs and water in varied ratios of 1:1, 1:2, 1:4, and 1:6 (in mL).

2.15.1. Mathematical Formulation. The models of the physiochemical properties were assessed through the following mathematical formulation.

2.15.1.1. Density Formulation.

$$p = m / V$$

where *p* is the density, *m* is the mass, and *V* is the volume of the AgNPs at varying temperature and water ratios of 1:1, 1:2, 1:4, and 1:6.

2.15.2. Specific Heat Equation.

$$q = mc\Delta T$$

where *q* is the heat energy, *m* is the mass, *c* is the specific heat capacity, and ΔT is the change in temperature of the AgNPs at varying temperature and water ratios of 1:1, 1:2, 1:4, and 1:6.

2.15.2.1. Thermal Conductivity via Heat Transfer.

$$K = (QL) / (A\Delta T)$$

where *K* is the thermal conductivity, *Q* is the amount of heat transferred, *L* is the distance between the two isothermal planes, *A* is the area of the surface, and ΔT is the difference in temperature of the AgNPs at varying temperature and water ratios of 1:1, 1:2, 1:4, and 1:6.

2.16. Computational Analysis. *2.16.1. Structural Prediction.* The primary amino acid sequences of PCR amplified genes, i.e., *spa*, *fmhA*, *hld*, and *LukD* was obtained through online tool ExPasy https://web.expasy.org/translate/. The tertiary structure was predicted by utilizing Phyre2 (http://www.sbg.bio.ic.ac.uk/phyre2/html/page.cgi?id=index). The AgNPs molecular construction with sub-atomic formula was retrieved from ChemSpider.

2.16.2. Structure Validation. The 3-D structures were further validated by running PROCHECK, Ramachandran Plot (https://www.ebi.ac.uk/thornton-srv/software/PROCHECK/).

2.16.3. Phylogenetic Tree Construction. Using the MEGA-X programme for phylogenetic analysis of specific molecular sequences, a phylogenetic tree was created to comprehend the evolutionary relationships between the genes of *S. aureus* and *S. argenteus*. Five homologous bacterial sequences were used to create the alignment and evolutionary relationship between the sequences.

2.16.4. Interactome Prediction. The Search Tool for the Retrieval of Interacting Genes (STRING) https://string-db.org/, which offers a database of known and expected protein interactions for 2 million proteins, was used to predict the interactome for the proteins *spa*, *fmhA*, *LukD*, and *hld*. This online tool allowed us to determine the structure, interactome, and activities of proteins that interact with other *S. aureus* and *S. argenteus* proteins.

2.16.5. Subcellular Localization. Using CELLO, an online programme that recognizes sorting signals and particular amino acid content in proteins, the subcellular localization of each protein was identified. This aids in evaluating the accuracy of the prediction.

2.16.6. Molecular Docking. Applying SwissDock (http://www.swissdock.ch/), it is allowing to predict the binding of two molecules in a preferred orientation to create a stable complex. Scoring functions may then be used to estimate the binding affinity or how strongly two molecules connect with one

another. Discovery Studio 3D Molecular Structure was used to visualize the docking.

2.16.7. 3-D QSAR Analysis. Quantitative structure–activity relationships (Cloud 3D-QSAR) in three dimensions are available at (http://chemyang.ccnu.edu.cn/ccb/server/cloud3dQSAR) allow for comparisons of a variety of molecular configurations and their biological effects on a specific target.

2.16.8. ADMET Analysis. Absorption, Distribution, Metabolism, Excretion, and Toxicity ADMET (www.swissadme.ch) used to analyze the attributes of clinical stages to predict the ADMET qualities is crucial to the drug design process.

3. RESULTS

3.1. Gene Amplification. The virulent and resistant genes, i.e., *Delta Hemolysin*, FmhA, *Spa* (proteinA), and *LukD* of
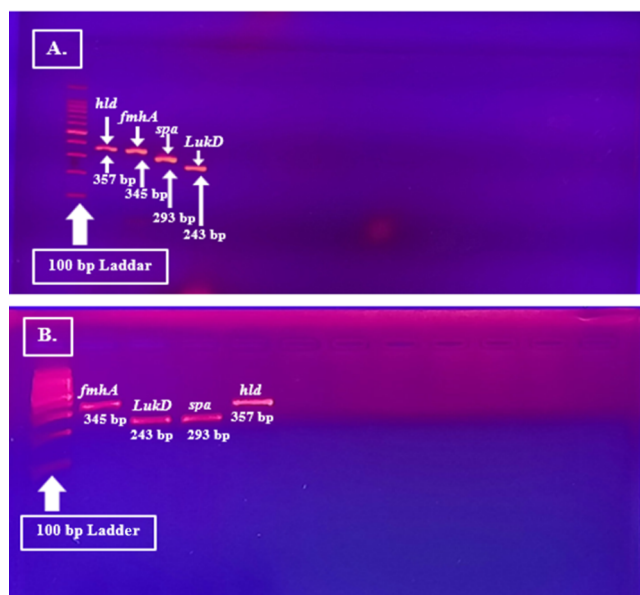
Figure 1. Amplification of virulence and resistance [Delta Hemolysin, *FmhA*, *Spa* (proteinA), and *LukD*], genes of (A) *S. aureus* and (B) *S. argenteus*.

molecularly characterized *S. aureus* and *S. argenteus* were amplified through PCR. *Delta Hemolysin*, *FmhA*, *Spa* (proteinA), and *LukD* genes present in different strains of *S. aureus* and *S. argenteus* were amplified with the product size of 357, 345, 293, and 243 bp, respectively as shown in Figure 1A,B. Gel electrophoresis was used to confirm genes by running on 2% gel.

3.1.1. Sequencing of Virulent and Resistance Genes. When the targeted virulent and resistance genes were amplified, they were sent for the ABI sequencing. Chromatograms showing the peaks of different targeted genes, as shown in Figure 2.

3.2. Phytochemical Screening of *C. harrisii*. The screened phytochemicals of leaves extract of *C. harrisii* are summarized in Table 2.

3.3. Determination of Reducing the Power of Leaves Extract of *C. harrisii*. The reducing power assay is based on the reduction mechanism of a substance that can potentially reduce potassium ferricyanide to potassium ferrocyanide. Potassium ferrocyanide then reacts further with ferric chloride to form a ferric–ferrous complex, which has maximum absorbance when measured at 700 nm (Figure 3). The reducing power of the leaf extract ($R^2 = 0.8538$) increases as its concentration increases,

demonstrating a good linear relationship of reducing Power in comparison to the control, ascorbic acid ($R^2 = 0.7964$).

3.4. Biosynthesis of Silver Nanoparticles. When precursor AgNO$_3$ was added to the leaves extract of *C. harrisii*, it reduced the Ag$^+$ to Ag^0, and a blackish brown color was observed when drop-wise precursor AgNO$_3$ was added to the leaves extract of *C. harrisii*; when increasing its incubation time, it reduces the Ag$^+$ ion to silver particles and thus shows the formation of AgNPs (Figure 4).

3.5. Characterization of AgNPs. *3.5.1. UV–Visible Spectrophotometry.* The absorbance of synthesized AgNPs was observed at 477 nm. This absorbance UV–vis spectra increases by increasing the incubation time. This graph shows that the Ag$^+$ to Ag^0 which indicated the peak of AgNPs as shown in the Figure 5.

3.5.2. Scanning Electron Microscopy. Surface morphology and molecule size of green integrated not set in stone by utilizing examining SEM. Normal filtering electron micrograph distinguishes that Ag NPs were very much scattered and round in shape (bead-like construction). In addition, average crystalline size obtained by Image J software for 25 mM AgNPs were viewed as 2.21 nm (Figure 6).

3.5.3. EDX Spectroscopy. EDX examination uncovered the basic creation of orchestrated nanoparticles. These metallic AgNPs express sharp top at 3 KeV because of its SPR which affirms the presence of silver particles and different components carbon, oxygen, and chlorine go about as diminishing and covering specialists (Figure 7). Examination shows non-attendance of nitrogen that guarantee total decrease of AgNO$_3$ into silver particles and no other follow particles are available in nanoparticles (Table 3).

3.5.4. FTIR Analysis. FTIR spectra indicate the surface structures and functional groups responsible for the reduction and stability of green-produced AgNPs. The peaks show different functional groups on the surface of the synthesized AgNP. It was determined that both symmetrical and asymmetrical C–O vibrational stretching were present based on the peak at 1007.55 cm^{-1}. The peaks confirmed the existence of aromatic chemicals in the leaves extract at 1502.10 and 1552.91 cm^{-1}. These peaks characterized by the FTIR spectroscopy confirm that all the functional groups that are the part of leaves extract and present on the surface of AgNPs play an efficient role as capping and reducing agents (Figure 8).

3.6. Antimicrobial Activity. The antimicrobial activities of AgNPs synthesized by *C. harrisii* and plant extract were studied with cefoxitin and vancomycin antibiotics. Different concentrations of AgNO$_3$ were used, and they showed the best results compared to antibiotics and plant extract. 0.25 M AgNO$_3$ shows the best results as compared to all other concentrations, 0.25 M shows a 20 mm zone of inhibition as compared to 1 M shows 8 mm, 0.1 M shows 12 mm, and plant extract shows a 16 mm zone of inhibition in *S. aureus* strain, but antibiotics show a minor zone of inhibition. Therefore, 0.25 M shows the best results, as shown below in Figure 9, and this concentration is further used for the characterization of the plant.

3.7. Anti-Inflammatory Activity. The maximum percentage inhibitions of protein denaturation were 99.15 and 97.46%, observed at 500 μg/mL concentration of AgNPs and leaves extract, respectively (Figure 10). The analyzed results interpreted that the synthesized AgNPs are more effective in inhibiting the denaturation of albumin protein than leaf extract and control drug (aspirin).
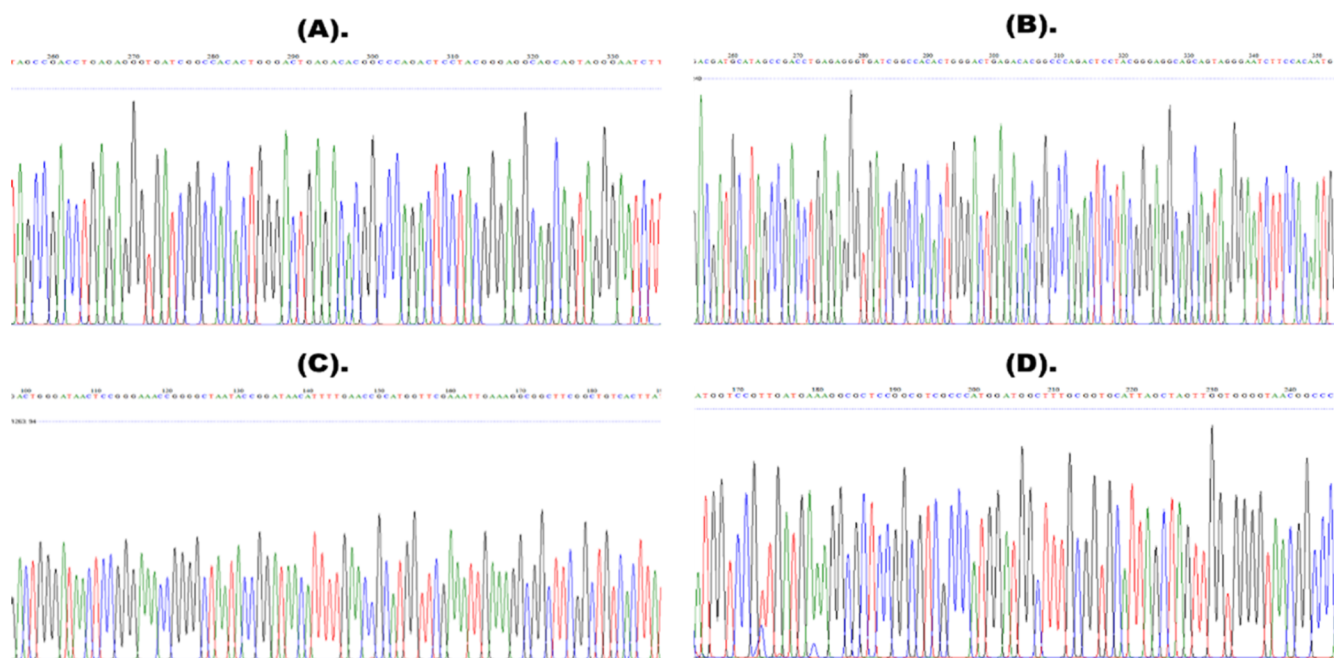
Figure 2. Chromatogram of different genes of *S. aureus* and *S. argenteus*, (A) *Delta Hemolysin* (B) *fmhA*, (C) *spa*, and (D) *LukD*.

Table 2. Phytochemically Screened Compounds Present in the Leaves Extract of C. harrisii

Sr #	phytochemical test	screened phytochemicals	interference	results
1	Wagner's test	alkaloids	a radish brown color appeared	present
2	foam test	saponins	stable foam formation	present
3	ferric chloride test	phenols	blue-green color appeared	present
4	Braymer's test	tannins	green precipitates formation	present
5	Salkowski's test	terpenoids	indication of yellow color with Salkowski's Test	present
6	Bontrager's test	quinones	red color appear in alkaline phase	present
7	Keller Killian's test	cardiac glycosides	pink to blood red color formation	absent
8	glycosides test	glycosides	appearance of pink color	absent
9	alkaline reagent test	flavonoids	yellow color appearance which becomes colorless when acid was added	present
10	precipitate test	phlobatannins	indication of red precipitates	present

3.8. Antioxidant Activity Analysis. The ability of the DPPH radical to reduce was assessed by the decrease in its absorbance at 517 nm caused by several antioxidants, i.e., the relationship between antioxidant compounds and radical advance, the scavenging of the radical via hydrogen donation is induced by the decrease in absorbance of the DPPH radical caused by antioxidants. The AgNPs showed the highest antioxidant activity of 99.8% at a maximum concentration of 1000 μg/mL (Table 4) (Figure 11).

3.9. Peptide Hemolytic Activity. After completing hemolytic activity, the results revealed that the activity was concentration dependent. The maximum concentration, 100 μg/mL, was used to obtain the greatest amount of hemolysis (89.9%). All lower doses showed less than 85% of hemolytic

activity, which earlier studies have shown to be safe for usage. Results based on hemolysis activity as a percentage indicated that nanoparticles at low concentrations were non-toxic and biocompatible. The usage of manufactured nanoparticles under uncontrolled circumstances might be harmful without evaluation of hemolysis activity (Figure 12).

3.10. Antidiabetic Activity. Less red color intensity in the alpha-amylase assay designated produced AgNPs as alpha-amylase enzyme inhibitors (Figure 13). The action was dose-dependent, increasing percent inhibition with the increase in concentration (200−1000 μg/mL) (45.24−90.56 percent). AgNPs show a 90.56% maximum inhibition, but metformin, a common medication, only shows a 71.99% maximum inhibition at the same dose (1000 μg/mL).

3.11. Cytotoxic Analysis. The dose-dependent killing of cells observed with cytotoxicity of drug increasing at lower concentrations for both cancer and non-cancer cell lines at various concentrations of AgNPs compared with positive and negative control (Figure 14).

3.12. Mathematical Models. *3.12.1. Density Parameter.* The density of AgNPs changes with the change in temperature and solvent accessibility ratio (Table 5). The mathematical model of density is represented in Figure 15 showing increase in density value of AgNPs with the increase in temperature and solvent.

3.12.2. Specific Heat Capacity. AgNPs' specific heat capacity varies as a function of temperature and the ratio of solvent accessibility (Table 6). Figure 16 illustrates the mathematical representation of heat capacity and the rise in AgNPs' specific heat capacity value with temperature and solvent.

3.12.3. Thermal Conductivity via Heat Transfer. Temperature and the ratio of solvent accessibility affect how well AgNPs transport heat, and these factors change their thermal conductivity (Table 7). Figure 17 shows the relationship between temperature and solvent on AgNPs' thermal conductivity value as well as the mathematical representation of thermal conductivity.

Reducing Power of Seed Extract Vs. Ascorbic Acid

$R^2 = 0.7964$
$R^2 = 0.8583$

	20 µl	40 µl	60 µl	80 µl	100 µl
Control	0.797	0.765	1.026	1.033	1.145
Leaves Extract	0.726	1.034	1.069	1.11	1.186

Concentration (µl)
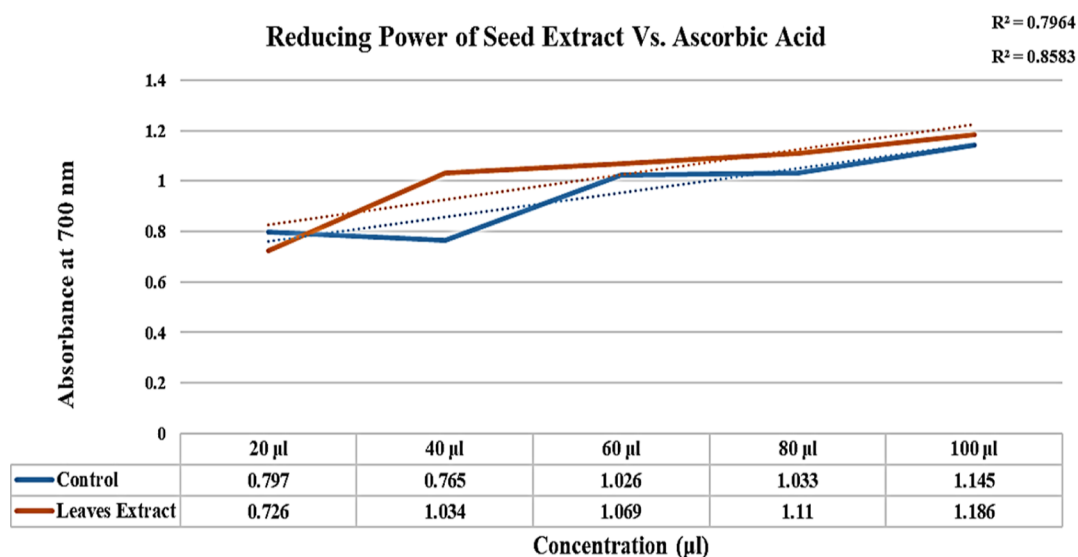
Figure 3. Determined reducing power of leaves extract with control, i.e., ascorbic acid showing the strong relationship, thus showing the capability of leaf extract to reduce the AgNPs.
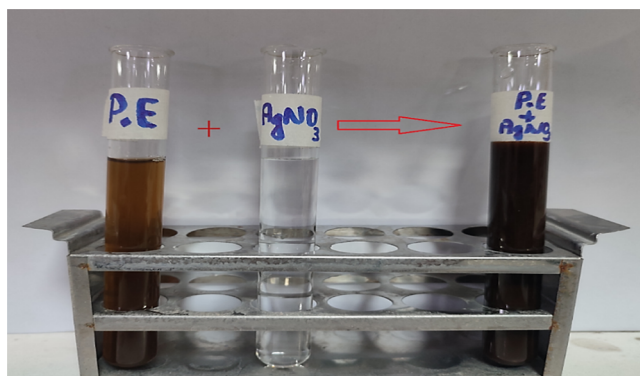
Figure 4. Plant's leaf extract transformation from pale orange to dark brown upon adding AgNO$_3$ precursor indicates the creation of AgNPs.
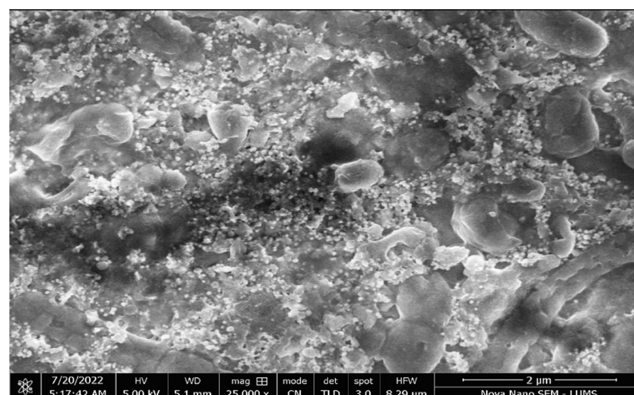
Figure 6. SEM micrograph of AgNPs synthesized by using the 25 mM solution of AgNO$_3$ and leaf extract of *C. harrisii.*

3.13. Computational 4.17 Analysis. *3.13.1. Structural Prediction.* The phyre2 anticipated the tertiary design of *spa,* fmhA, *LukD,* and hld with 81, 96, 81, and 9% grouping

personality with QMEAN Z-Scores of −0.69, −0.89, −0.79, and −1.12, respectively. The scoring list and other relatable variables showed the protein structure as higher certainty expectation.

UV-Vis Spectrophotometry
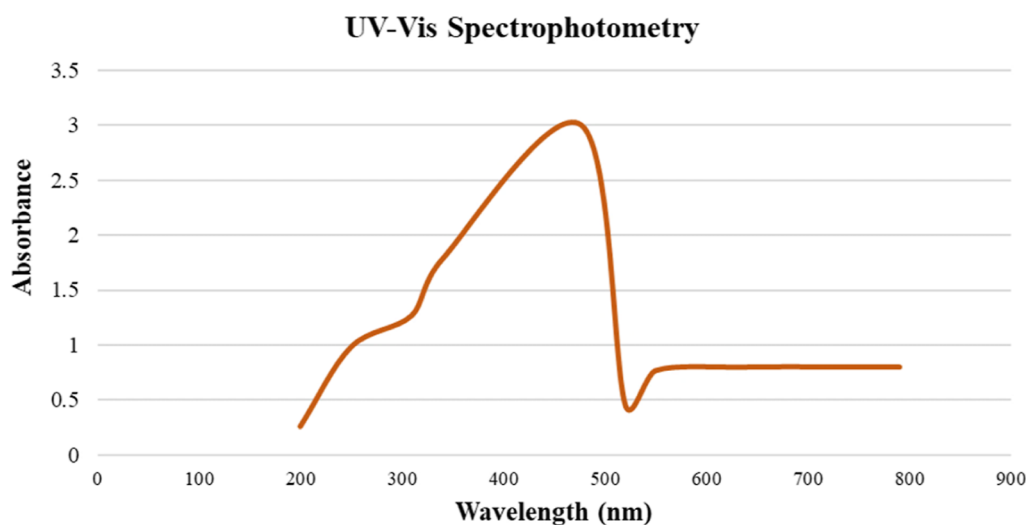
Figure 5. UV−visible spectrophotometry of AgNO$_3$ that was synthesized using *C. harrisii* leaf extracts from a 0.25 M precursor solution of AgNO$_3$.
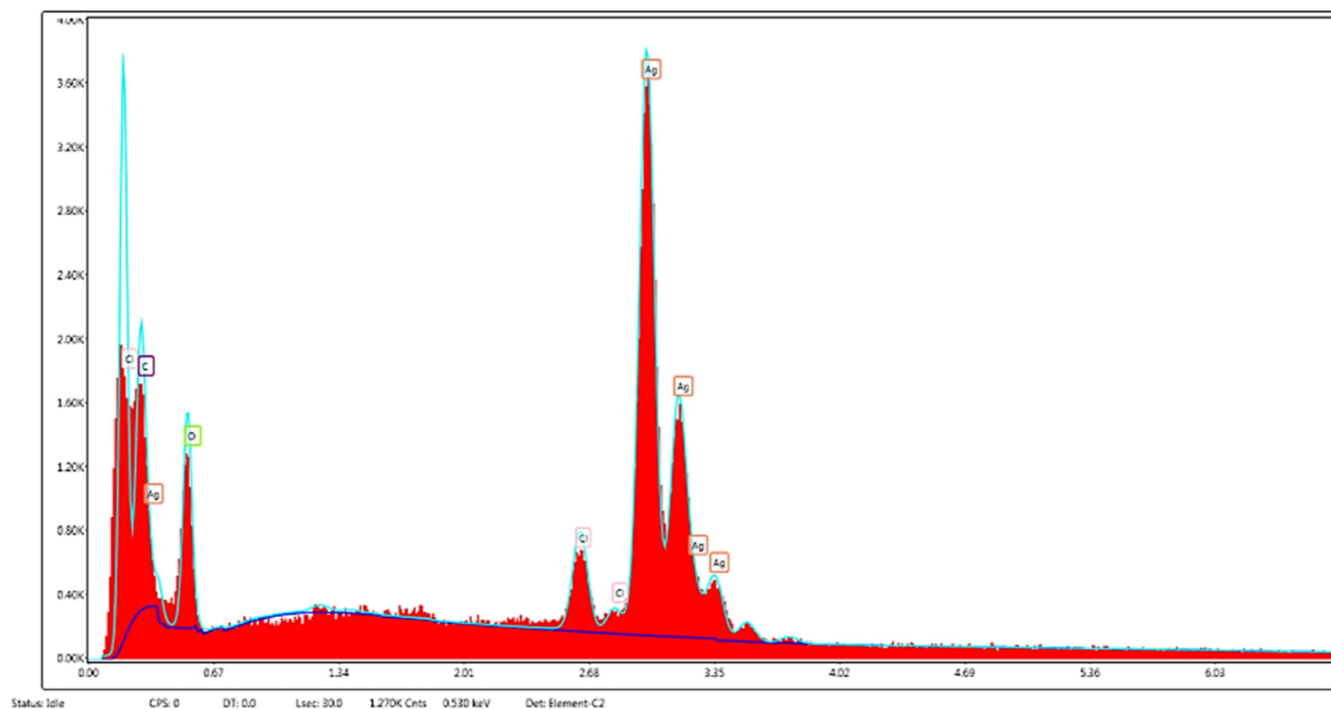
Figure 7. EDX spectrum of AgNPs depict Ag peak in between 2 and 3 KeV.

Table 3. Elemental Composition of Synthesized Silver Nanoparticles

element	weight %	atomic %	net int
C K	4.55	20.02	253.82
O K	10.32	34.04	253.12
ClK	4.29	6.39	166.52
AgL	80.84	39.56	1253.12

The quality assessment determined by Phyre2 was additionally in the ideal and standard reach. Accordingly, the construction was on the quality norms and significant for the utilization of docking study and different purposes. The anticipated tertiary
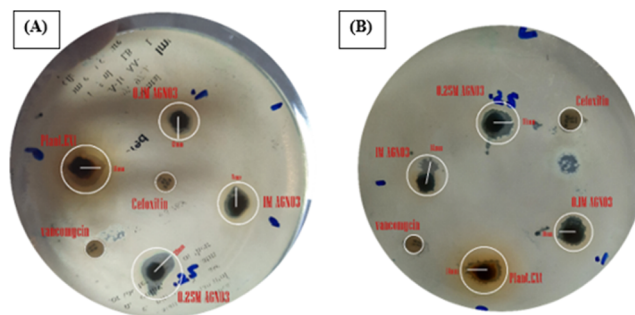
Figure 9. Antimicrobial activity comparison with nanoparticle (a) *S. aureus* and (b) *S. argenteus.*
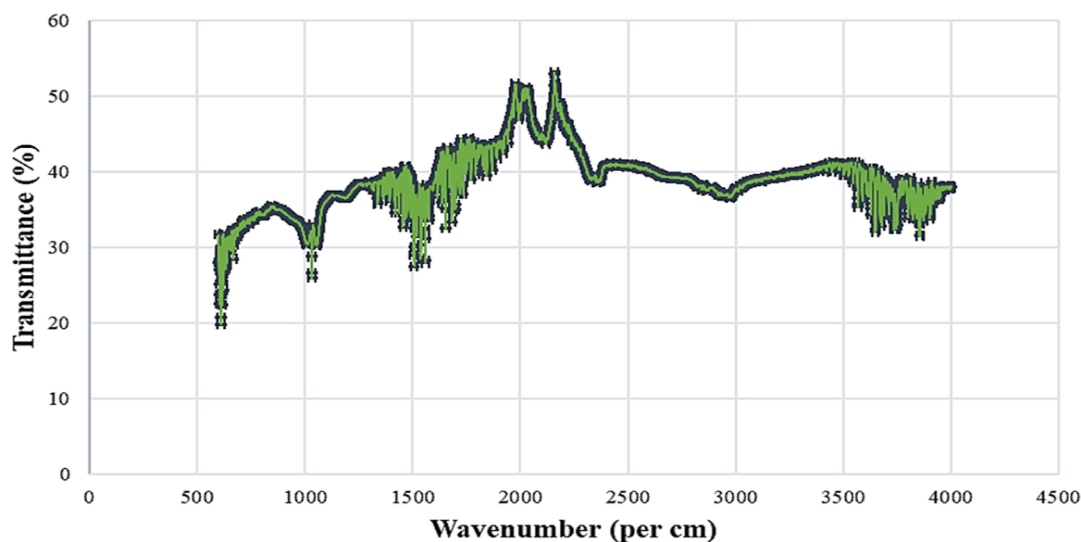
Figure 8. FTIR analysis of AgNPs synthesized by leaves extract of *C. harrisii.*
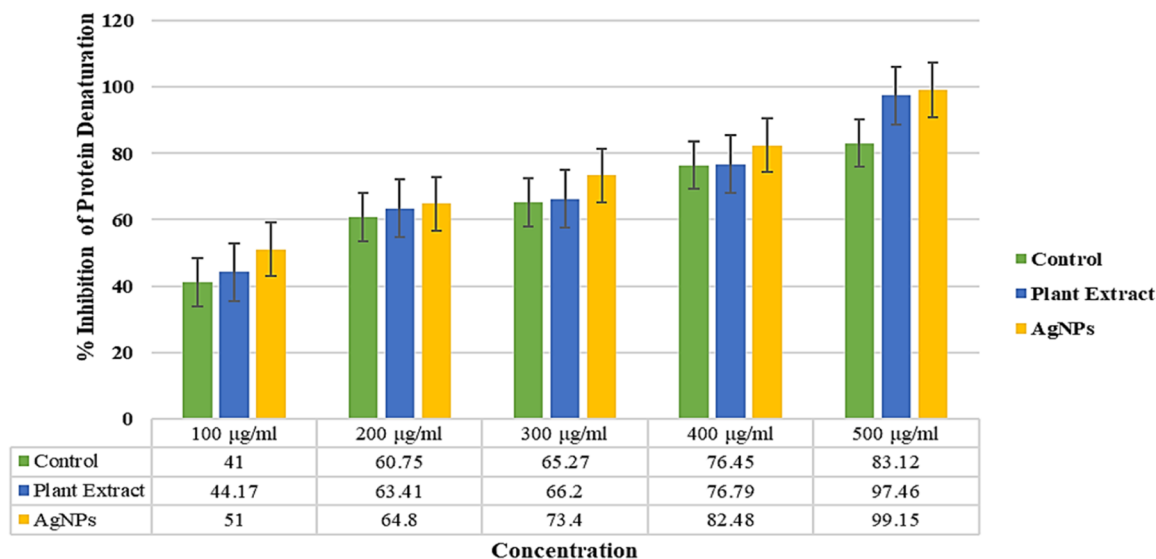
Figure 10. Graphical presentation of % inhibition of protein denaturation at specific concentrations of control (aspirin), leaf extract, and AgNPs, thus showing 99.15% anti-inflammatory activity by AgNPs at 500 μg/mL.

Table 4. Antioxidant Activity of Plant Extract and AgNPs Compared with Control at (517 nm)

	antioxidant activity (517 nm)					
	% free radical scavenging			IC50		
concentration (μg/mL)	ascorbic acid	leaves extract	AgNPs	ascorbic acid	seed extract	AgNPs
200	3	9.5	24.34	599.9040594	594.7754605	594.9177
400	55.48	57.32	58.38			
600	64.3	71.77	76.52			
800	70.9	80.21	82.25			
1000	85.45	86.61	99.8			
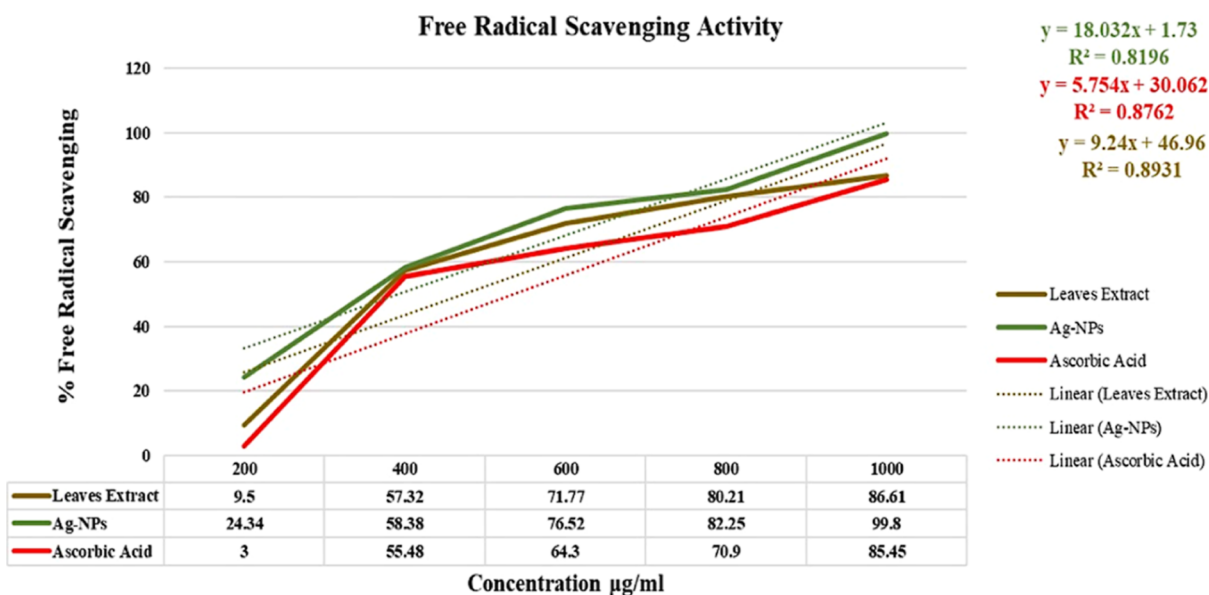
Figure 11. Graphical representation for the antioxidant activity showing the highest scavenging percentage of AgNPs (99.8%) at 1000 μg/mL concentration.

construction of *spa*, fmhA, *LukD*, and hld is given underneath in Figure 18.

3.13.2. 3-D Structure Validation. To evaluate the more primary approval and nature of the built tertiary design, the

Ramachandran plot was developed to figure out the points and Rama inclined toward areas in the structure. The buildups in the Rama most preferred locales were determined as around 90% for each of the three-dimensional designs, and the deposits in the

Anti-Hemolysis Activity

Concentration	20 μg/ml	40 μg/ml	60 μg/ml	80 μg/ml	100 μg/ml
Control	82.23	82.23	82.23	82.23	82.23
Plant Extract	13.75	14.28	14.28	23.52	13.9
AgNPs	19.25	22.45	13.9	17.64	9.6
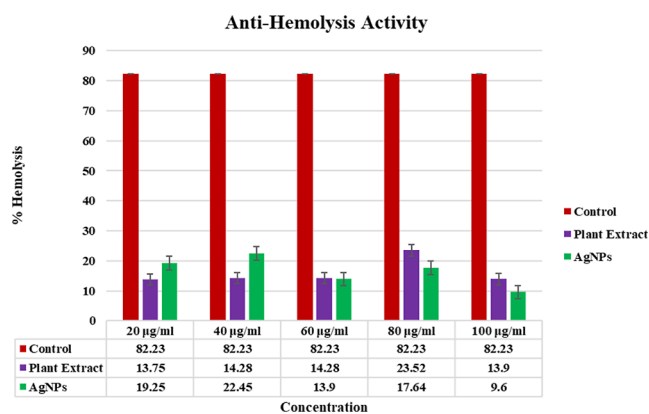
furthermore permitted districts were determined as around 9% (Figure 19). Albeit the deposits in liberally prohibited areas were figured as 0.4% and the buildups in refused districts were 0.6%. The consequences of Ramachandran plot portrayed the design as of good quality and dependable for any sort of utilization in the trial and error and examination.

3.13.3. Phylogenetic Tree Construction. The MEGA-X explained the genealogical relationship of *spa*, *LukD*, *hld*, and *fmhA* qualities and the outcomes portrayed that all qualities has imparted the familial start to different stains of *S. aureus*. Albeit, a nearby genealogical relationship was seen in the *S. aureus* and *S. argenteus.*. Figure 20 underneath shows the local joining trees built by MEGA-X at the bootstrap worth of 1000.

3.13.4. Interactome Prediction. Subsequent to creating the interactome of *spa*, *LukD*, *fmhA*, and *hld* protein, the outcomes showed that proteins of interest associate with different proteins

$y = 11.848x + 30.42$
$y = 11.449x + 23.681$
$y = 11.094x + 19.142$

Anti-Diabetic Activity (540 nm)

Concentration μg/ml	200 μg/ml	400 μg/ml	600 μg/ml	800 μg/ml	1000 μg/ml
Ag-NPs	45.24	51.38	63.42	79.22	90.56
Leaves Extract	38.09	44.02	55.59	70.19	82.25
Control	30.15	40.97	50.78	68.23	71.99
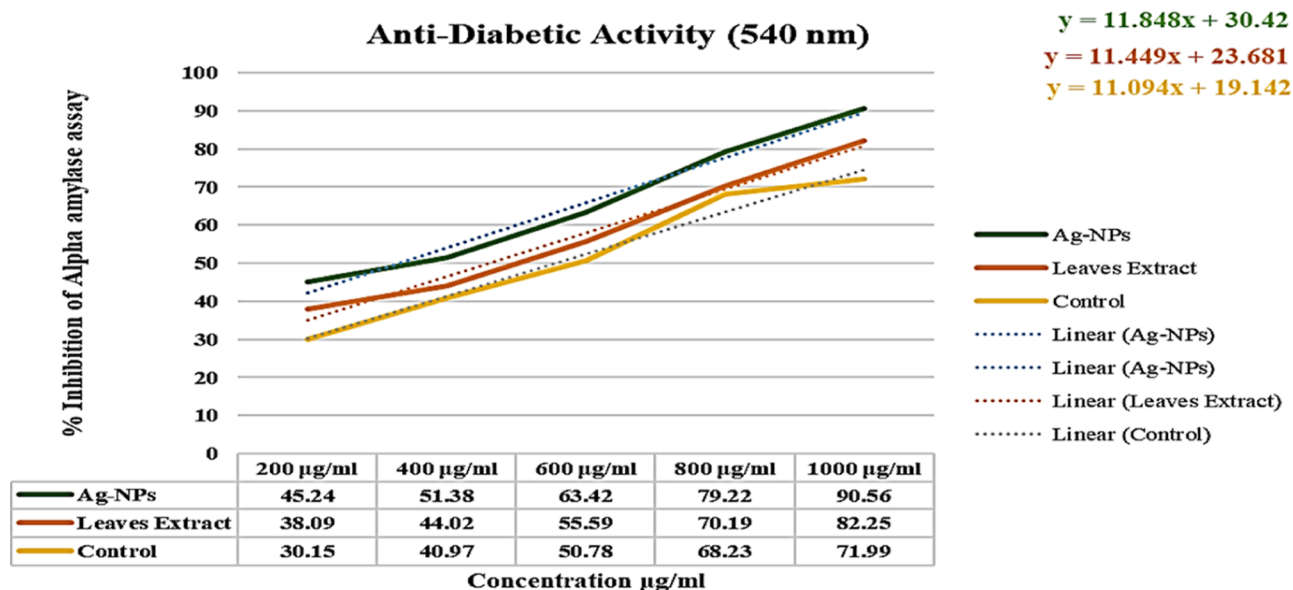
Figure 13. Graphical representation of antidiabetic activity showing 90.56% inhibition of alpha amylase assay by AgNPs.

Cytotoxic Analysis

Concentration	800	600	400	200	100	50	Negative control	Doxorubicin
W1- HEK293	143.5707599	105.53995	51.34031146	38.37202	42.51553059	31.0696962	92.69849	82.2594
W1-U87	289.6481	149.8728177	97.092149	54.95818399	51.88461094	38.51119	101.81331	59.8512
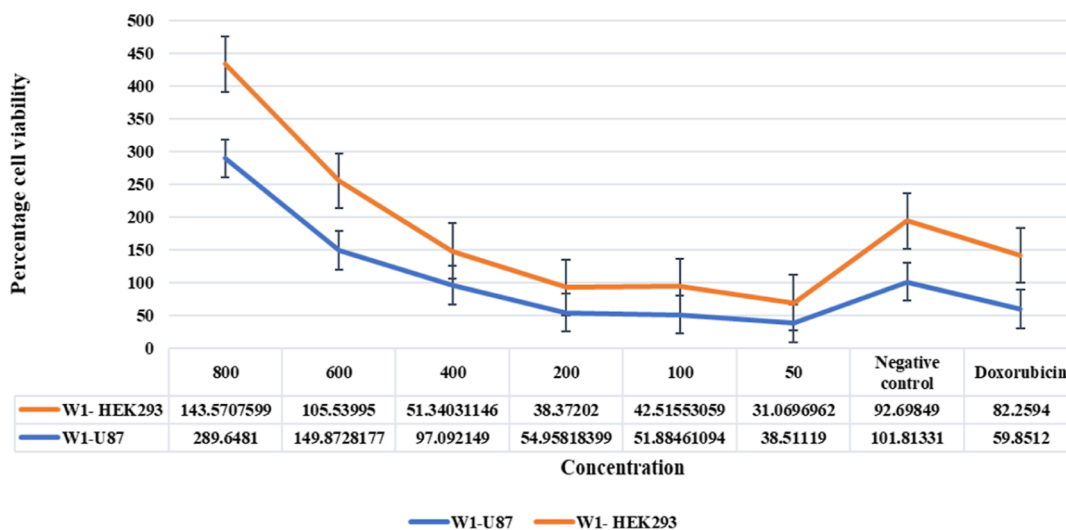
Figure 14. Cell viability of compound W1 on HEK 293 and U87 cell lines on 24 h. There was a dose-dependent killing observed with the cytotoxicity of drug increasing at lower concentrations for both cancer and non-cancer cell lines.

Table 5. Variation in Density (kg/m³) as a Function of Solvent Content and Temperature[a]

temperature (°C)	ρ^{1b}	ρ^{2b}	ρ^{3b}	ρ^{4b}
15	82	143.33	152.28	160.21
20	75.45	290.43	300.45	310.25
25	67.67	369.28	360.82	365.28
30	59.14	299.45	290.58	280.65
35	70.96	480.58	470.23	490.12
40	66.51	585.24	530.54	570.45

[a]ρ^{1b} = density of AgNPs; ρ^{2b}, ρ^{3b}, and ρ^{4b} = density after mixing nanoparticles and water in the ratios 1:2, 1:4, and 1:6 (in mL).
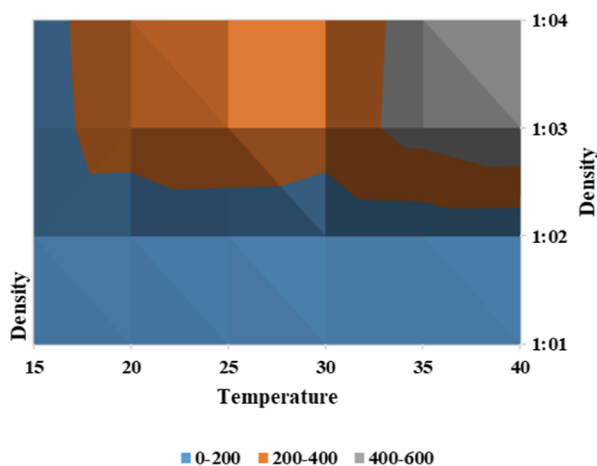
Figure 15. Density profiling of AgNPs at the ratio 1:1, 1:2, 1:4, and 1:6 of the water.

Table 6. Variation of the Nanofluid's Specific Heat (J/K/ mol) with Temperature and the Volume of Solvents[a]

temperature (°C)	ρC^p	ρC^{p2}	ρC^{p3}	ρC^{p4}
15	350	400	600	660
20	280	600	500	350
25	500	800	900	950
30	660	1000	1500	1050
35	980	1400	1250	1850
40	820	1200	1450	1550

[a]ρC^{p1} = Specific heat capacity of AgNPs; ρC^{p2}, ρC^{p3}, and ρC^{p4} = Specific heat of AgNPS after mixing nanoparticles and water in 1:2, 1:4, and 1:6 (in mL).

which are principally limited in the nucleus, plasma membrane, and some of them are found in extra-cellular *spa*ce. As the quantity of communications high, in the wake of producing interactome utilizing STRING on the web device, simply the most elevated certainty associations were picked for additional examination in this review, while medium and low certainty were discarded (Figure 21).

Subsequent to creating the interactome of *spa*, *LukD*, fmhA, and hld protein, the outcomes showed that proteins of interest associate with different proteins which are principally limited in the nucleus, plasma membrane, and some of them are found in the extracellular *spa*ce. As the quantity of communications high, in the wake of producing interactome utilizing STRING on the web device, simply the most elevated certainty associations were
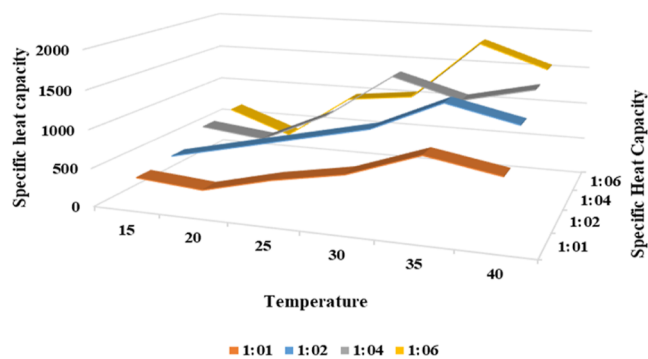
Figure 16. Mathematical model of specific heat capacity of AgNPs at a particular temperature range of (15−40 °C) along with the solvent mixing at 1:1, 1:2, 1:4, and 1:6.

Table 7. How Thermal Conductivity (Knf) Varies with Temperature and Solvent Concentration[a]

temperature (°C)	Knf¹	Knf²	Knf³	Knf⁴
15	410.65	1159.31	1165.18	1178.25
20	208.63	920.38	949.67	965.14
25	620.55	2820.94	2820.96	2797.51
30	408.21	2546.11	2557.43	2524.28
35	520.98	4374.68	4352.24	4374.45
40	120.4	5582.8	5520.21	5598.49

[a]Knf¹ = Thermal conductivity of AgNPs; Knf², Knf³, and Knf⁴ = thermal conductivity of ZVI-NPs after mixing nanoparticles and water in 1:2, 1:4, and 1:6 (in mL).
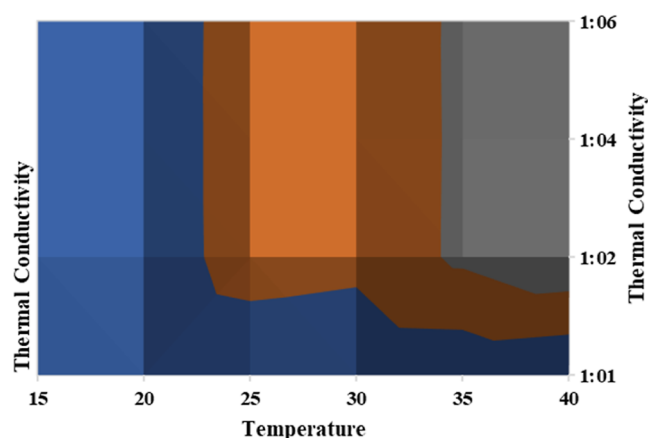
Figure 17. Mathematical model of thermal conductivity of AgNPs at a particular temperature range of (15−40) along with the solvent mixing at 1:1, 1:2, 1:4, and 1:6.

picked for additional examination in this review, while medium and low certainty were discarded (Figure 21).

3.13.5. Subcellular Localization. The subcellular localization determined that *fmhA* and *hla* are located in cytoplasmic fluid, *spa* is located in the extracellular matrix, and *LukD* is located in outer membrane *spa*ce of the bacteria cell with high prediction scores of 2.032, 2.582, 1.635, and 2.499, respectively (Table 8).

3.13.6. Molecular Docking. SwissDock was used to check the binding affinity of the AgNPs with the predicted proteins, i.e., *spa*, *LukD*, fmhA, and hld. The best interaction energy of AgNPs
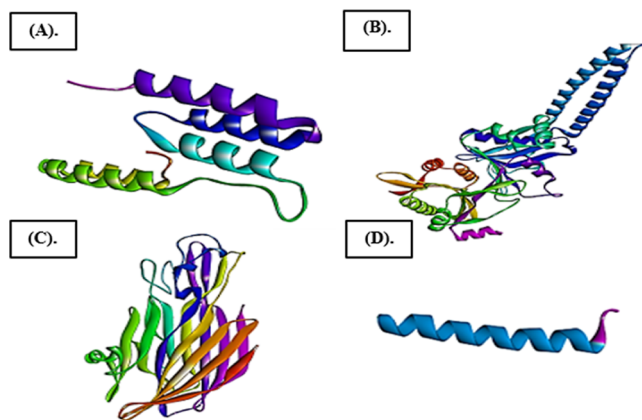
Figure 18. 3-D structure prediction of the amplified genes via Phyre2. (A) *Spa*, (B) fmhA, (C) *LukD*, and (D) *hld.*

with *spa* was −7.16 (Figure 22A), with *LukD* was −6.5 (Figure 22B), with fmhA was −6.45 (Figure 22C) and with hld was −3.3 (Figure 22D). The visualization of 2-D and 3-D docking interactions was done via Discovery studio. Therefore, many studies are to be conducted regarding hld as it shows the least binding affinity with AgNPs due to its small size in nature.

3.13.7. 3-D QSAR Analysis. Three-dimensional quantitative structure–activity relationships (Cloud 3D-QSAR) permit a good q^2 and r^2 score of the docking complexes. The q^2 and r^2 scores of *spa* protein and AgNP complex are 0.9987 and 0.9228, scores of *LukD* and AgNPs complex are −0.3439 and 0.995, and scores of fmhA and AgNPs complex are 0.8254 and 0.9646, while scores of hld are 0.891 and −0.987, respectively (Figure 23).

3.13.8. ADMET Analysis. ADMET analysis showed that ligand AgNPs used as drug for the accessibility of the amplified genes are biocompatible and readily available for the neutralization of the virulent genes of the pathogenic bacteria, i.e., *S. aureus* and *S. argenteus* (Figure 24).

4. DISCUSSION

S. aureus is a Gram-positive, spherical bacterium from the Firmicutes family. The majority of this microbiota may be found in the top and dermal layers of the body. Researchers have found that the majority of the bacteria that cause infections are multidrug resistant. In addition to MRSA and multidrug-resistant *Streptococcus pneumoniae*, other bacteria such as *Mycobacterium tuberculosis* are becoming increasingly difficult to treat. There are cases when these bacteria are beneficial because they are believed to be the microbiome of our bodies. It causes pneumonia and drug resistance when these bacteria go out of control.[16] To counteract antibiotic effects, microorganisms use mechanisms controlled by cells to evade antibiotic targets. Antibiotics can fit into the active site of the bacteria for a short period of time. Antibiotics become less effective because of this inhibition. Antibiotic resistance is turning endangered species into extinct ones. Antibiotic resistance is being pushed forward because of widespread misuse. Antibiotic use and the emergence of novel bacterial strains go hand in hand.[17]

Antibiotics are a highly effective weapon that has been developed to combat the micro world. To counteract antibiotic effects, microorganisms use mechanisms controlled by cells to evade antibiotic targets. Antibiotics become less effective as a result of this inhibition. Antibiotic resistance is being pushed forward as a result of widespread misuse. Bacterial mutations, horizontal gene transfer, or cis gene transfer all contribute to the evolution of resistance in distinct bacterial strains.[18] There is a pressing need for innovative therapies, and homoeopathy is one of such treatments. The treatment of a sickness in a homoeopathic manner is accomplished by treating the patient with the chemicals that cause that ailment. The term homoeopathy refers to the practice of assisting the body's natural ability to heal itself. When a person is unwell, they are given medicine that helps them self-heal, and this is how it works.[19]
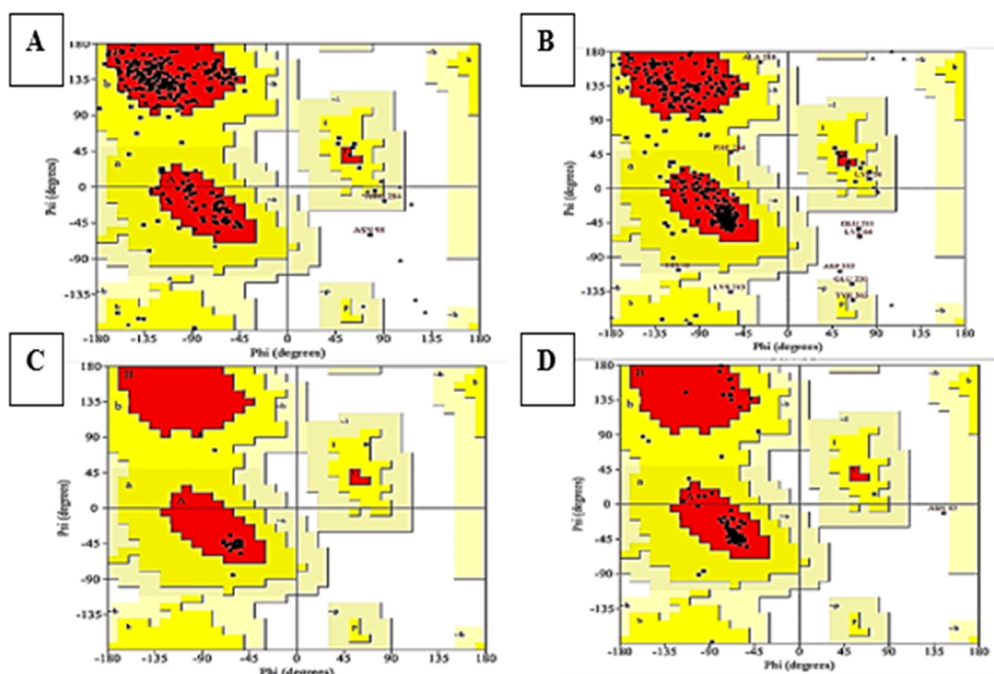
Figure 19. 3-D structure validation by Ramachandran Plot of ROCHECK. (A) *Spa*, (B) fmhA, (C) *LukD*, and (D) hld.
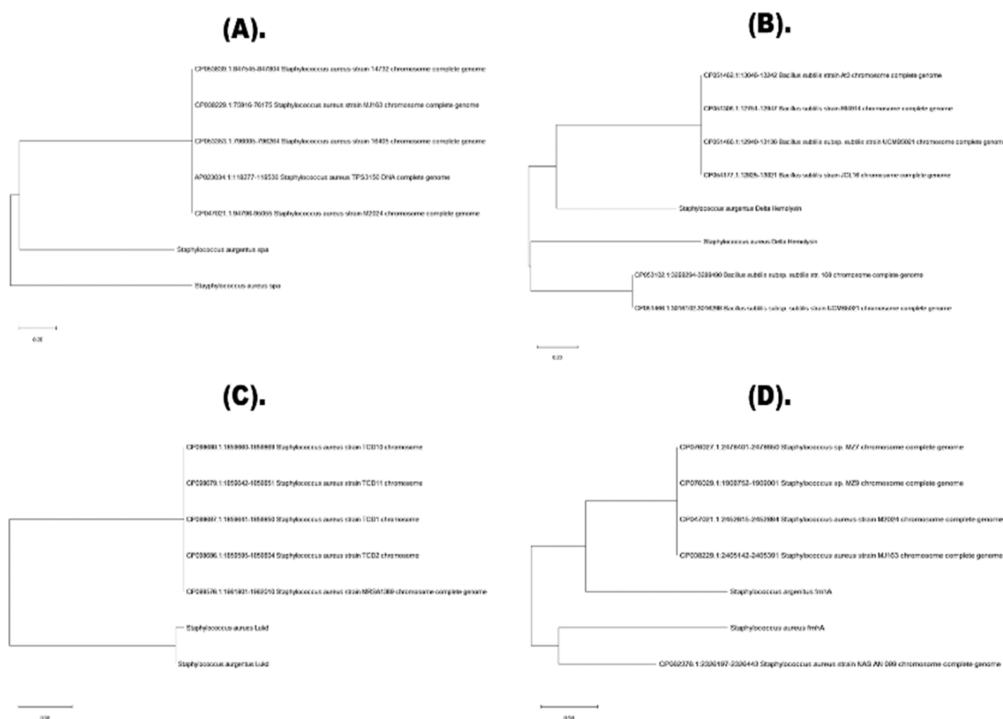
Figure 20. Phylogenetic analysis of the amplified genes via MEGA-X. (A) *spa*, (B) *hld*, (C) *LukD*, and (D) *fmhA*.
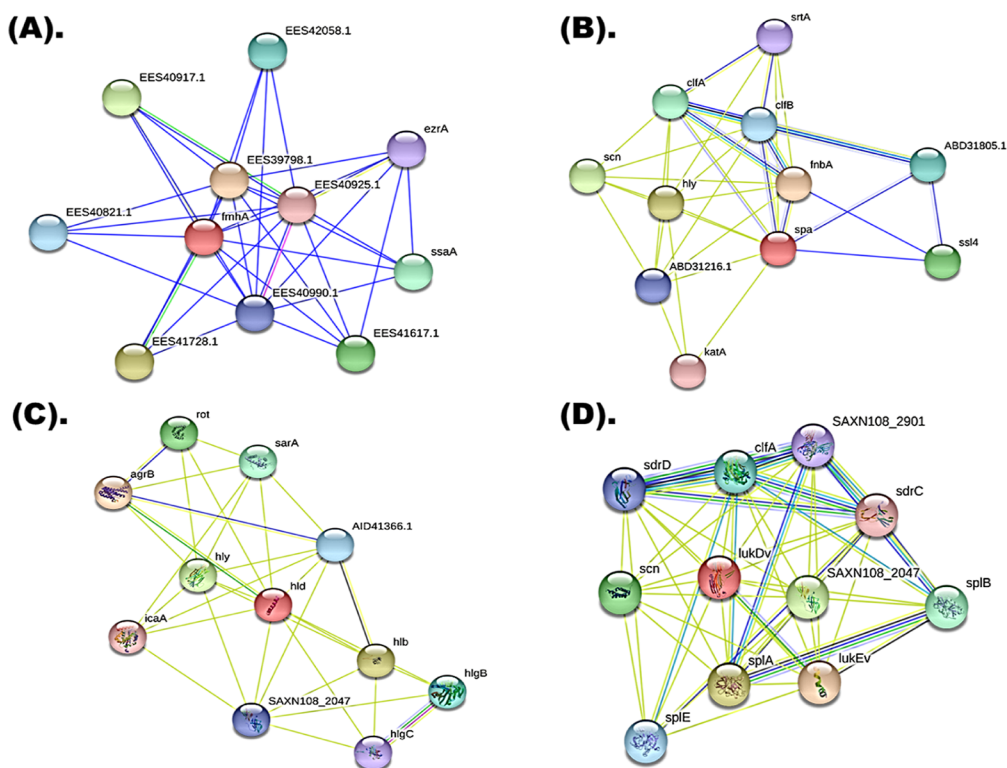
Figure 21. Interactome prediction through STRING. (A) *fmhA*, (B) *spa*, (C) *hld*, and (D) *LukD*.

Table 8. Subcellular Localization of the Amplified Genes via CELLO

gene name	cello prediction	prediction score
FmhA	cytoplasmic	2.032
Spa	extracellular	1.635
LukD	outer membrane	2.499
Hld	cytoplasmic	2.582

In this study, samples of MRSA were taken from Sheikh Zayed Hospital and different biochemical tests were applied for the identification of pure strains of MRSA. All the strains showed a positive catalase test, strain two ST2 showed positive gelatinase test but ST1 and ST3 resulted negative, while ST1 and ST2 came positive for NaCl tolerance test and ST3 resulted negative. The sugar fermentation test carried out against lactose, sucrose,
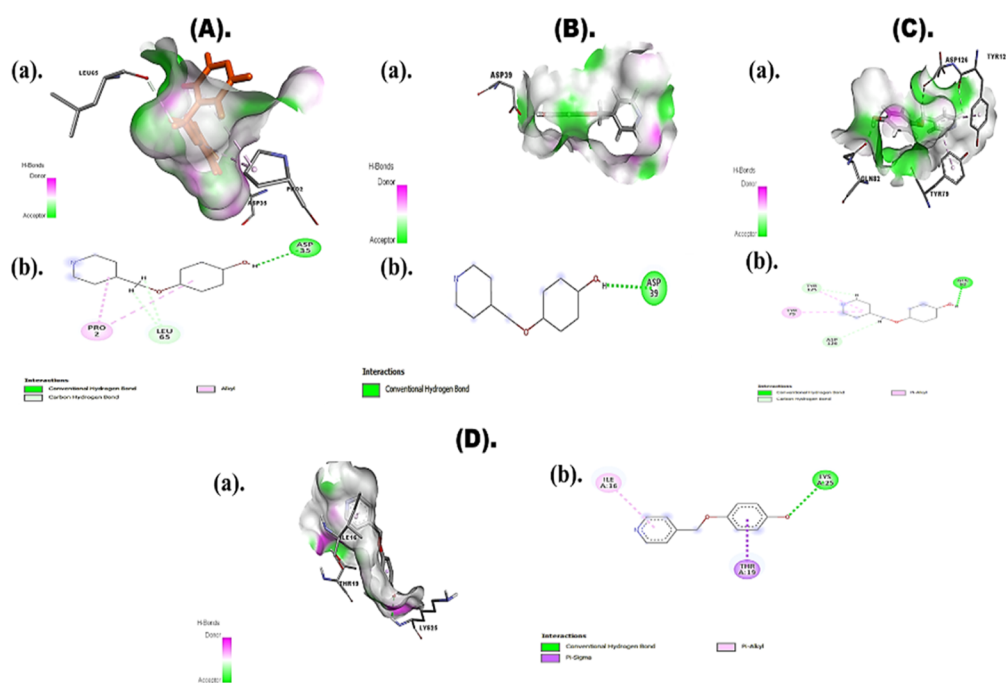
Figure 22. Docking analysis of AgNPs with amplified virulent genes: (A) *spa*: (a) 3-D complex and (b) 2-D complex; (B) *LukD*: (a) 3-D complex and (b) 2-D complex; (C) *fmhA*: (a) 3-D complex and (b) 2-D complex; and (D) *hld*: (a) 3-D complex and (b) 2-D complex.
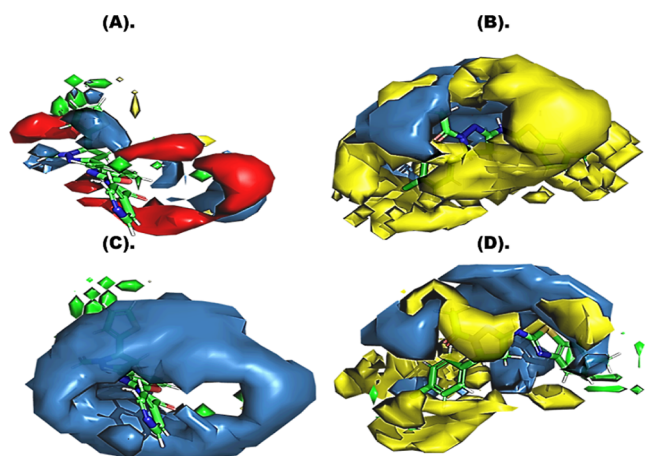
Figure 23. 3-D QSAR analysis of docked complexes. (A) *spa*, (B) *LukD*, (C) fmhA, and (D) hld.

and galactose and all three sugars resulted positive. The CTAB procedure was used to extract DNA, which was then verified by passing it through a 1% gel and looking at it under a Gel Dock. A 1 Kb ladder was used to amplify the 16S rRNA gene sequences during the PCR step. The amplified area had a size of 1400 bp, and bands were validated by running on a 2% Gel solution. *S. aureus* and *S. argenteus* findings from samples of gel electrophoresis delivered to ABI (applied bioscience) Company of Malaysia for sequencing were verified and published to NCBI Genbank. Virulence genes like Delta Hemolysin, *FmhA*, *Spa* (proteinA), and *LukD* of *S. aureus* were amplified with product sizes of 357, 345, 293, and 243 bp, respectively.[16] The leaves of the plant *C. harrisii* collected, dried, ground, and filtered their solution using filter paper and stored at 4 °C in the lab refrigerator to use further for the synthesis of silver nanoparticles, phytochemical screening, and determination of reducing the power of *C. harrisii*. There is a good linear

association between ascorbic acid (R^2 = 0.7964) and the reduction power of the leaf extract (R^2 = 0.8538) as the concentration of the leaf extract increases. The phytochemicals screening of plant extract through a number of tests interpreted that almost all the phytochemical present in plant extract except cardiac glycosides and glycosides.[20]

Anti-inflammatory activity of *C. harrisii* leaves extract and greenly synthesized AgNPs observed through protein denaturation. At 500 g/mL AgNPs and leaf extract, protein denaturation inhibited 99.15 and 97.46%, respectively, and NPs are more effective than the drug and leaf extract. The AgNPs showed the highest antioxidant activity of 99.8% at a maximum concentration of 1000 μg/mL. Antimicrobial activity of *C. harrisii* AgNPs and plant extract was tested using cefoxitin and vancomycin. AgNO$_3$ demonstrated better outcomes than antibiotics and plant extracts. 0.25 M AgNPs displays a 20 mm zone of inhibition compared to 1 M's 8 mm, 0.1's 12 mm, and plant extract's 16 mm in *S. aureus* strain; however, antibiotics show modest zones of inhibition. 0.25 M for the rest.

The recent investigation showed that AgNPs significantly harmed the cancer cell lines HEK 293 and U87. As the amount of AgNPs grew, the percentage of viable cells fell. The anticancer potential of Pechuelloeschea leubnitziae extract- AgNPs against the U87 glioblastoma cell line was demonstrated by the extract's concentration-dependent anti-proliferative activity. The relevance of our findings was further supported by the cytotoxic effects of AgNPs mediated by *C. harrisii* on the HEK 293 cell line. They proposed that the dosage concentration affects cell viability.

With QMEAN Z-Scores of −0.69, −0.89, −0.79, and −1.12 independently, the phyre2 predicted the tertiary design of *spa*, *fmhA*, *LukD*, and *hld* with 81, 96, 81, and 99% grouping personalities. MEGA-X described the ancestry of the *spa*, *LukD*, hld, and fmhA traits, and the results showed that each gene had given rise to a particular stain of *S. aureus*. The results of building the interactome of the proteins *spa*, *LukD*, *fmhA*, and *hld*
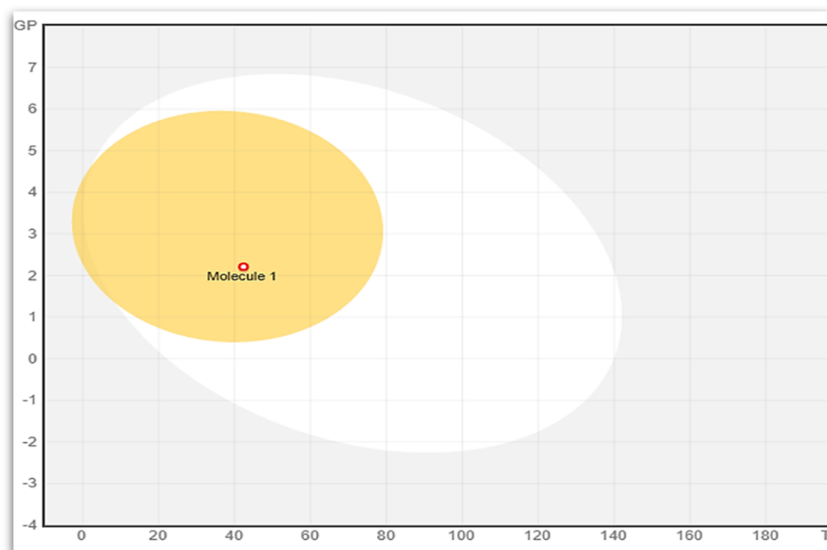
Figure 24. Boiled egg showing that our nanoparticle molecule is BBB-permeant and is not a substrate of PGP, hence making it efficient enough to work in the CNS.

revealed that the proteins of interest connect with several other proteins, many of which are restricted to the nucleus, plasma membrane, and others of which are located in extracellular *spa*ce. With high prediction scores of 2.032, 2.582, 1.635, and 2.499, respectively, the subcellular localization revealed that *fmhA* and *hld* are situated in cytoplasmic fluid, *spa* is found in the extracellular matrix, and *LukD* is located in outer membrane *spa*ce of the bacterium cell.[21]

SwissDock was employed to determine the AgNPs's affinity for the anticipated proteins *spa*, *LukD*, fmhA, and hld. AgNPs's best interaction energies were −7.16 with *spa*, −6.5 with *LukD*, −6.45 with *fmhA*, and −3.3 with *hld*. Quantitative structure−activity relationships in three dimensions (Cloud 3D-QSAR) enable the docking complexes to achieve high q^2 and r^2 scores. *Spa* protein and the AgNP complex have q^2 and r^2 scores of 0.9987 and 0.9228, scores of *LukD* and the complex are −0.3439 and 0.995, scores of *fmhA* and the complex are 0.8254 and 0.9646, and scores of *hld* are 0.891 and −0.987, respectively. The present, first-ever biosynthesis of nanoparticles from *C. harrisii* leaves extract explores the viability of green synthesis in the realm of nanotechnology.

5. CONCLUSIONS

The serious issue of multi-drug resistance in bacterial pathogens is linked to the high rates of sickness and mortality among living things as a result of elevated beta-lactamase levels. In the fields of science and technology, plant-derived nanoparticles have become very important for combating bacterial illnesses, particularly multidrug-resistant pathogens. The *spa*, *LukD*, *fmhA*, and hld genes were found when *S. aureus* and *S. argenteus* were characterized using PCR. Utilizing the leaf extract of *C. harrisii*, whose metabolites serve as capping and reducing agents for precursors of nano-synthesis, the green synthesis of AgNPs was carried out. EDX, SEM, FTIR, X-ray diffraction, and UV−vis spectroscopy were used to characterize the synthesized AgNPs. When compared to the antibiotics vancomycin and cefoxitin, along with the crude plant extract, AgNPs' antibacterial activity demonstrated a 20 mm inhibition of *Staphylococcus* species, whereas these other agents only showed a modest zone of inhibition. The interaction of the amplified

genes (*spa*, *LukD*, *fmhA*, and *hld*) with AgNPs was also examined computationally at the molecular level. AgNPs bound to *spa*, *LukD*, *fmhA*, and *hld* with binding affinities of −7.16, −6.50, −6.45, and −3.3 kJ/mol, respectively, indicating high docking scores with the exception of *hld*, which is −3.3 kJ/mol due to its tiny size. The key characteristics of biosynthesized AgNPs have shown to be a successful strategy for future drug-resistant *Staphylococcus* species control.

■ AUTHOR INFORMATION

Corresponding Authors

Muhammad Naveed − *Department of Biotechnology, Faculty of Science and Technology, University of Central Punjab, Lahore 54590, Pakistan*; Email: dr.naveed@ucp.edu.pk

Tariq Aziz − *Department of Agriculture, University of Ioannina, Arta 47100, Greece*; ⊙ orcid.org/0000-0003-0905-8076; Email: iwockd@gmail.com

Authors

Muhammad Waseem − *Department of Biotechnology, Faculty of Science and Technology, University of Central Punjab, Lahore 54590, Pakistan*

Shafiq ur Rehman − *Department of Basic and Applied Chemistry, Faculty of Science and Technology, University of Central Punjab, Lahore 54000, Pakistan*

Syeda Izma Makhdoom − *Department of Biotechnology, Faculty of Science and Technology, University of Central Punjab, Lahore 54590, Pakistan*

Metab Alharbi − *Department of Pharmacology and Toxicology, College of Pharmacy, King Saud University, Riyadh 11451, Saudi Arabia*

Abdulrahman Alsahammari − *Department of Pharmacology and Toxicology, College of Pharmacy, King Saud University, Riyadh 11451, Saudi Arabia*

Abdullah F. Alasmari − *Department of Pharmacology and Toxicology, College of Pharmacy, King Saud University, Riyadh 11451, Saudi Arabia*

Complete contact information is available at:
https://pubs.acs.org/10.1021/acsomega.3c01597

■ REFERENCES

(1) Varela, M. F.; Stephen, J.; Lekshmi, M.; Ojha, M.; Wenzel, N.; Sanford, L. M.; Hernandez, A. J.; Parvathi, A.; Kumar, S. H. J. A. Bacterial resistance to antimicrobial agents. *Sci. Prog.* **2021**, *10*, 593−622.

(2) Bush, K.; Bradford, P. A. Interplay between β-lactamases and new β-lactamase inhibitors. *Nat. Rev. Microbiol.* **2019**, *17*, 295−306.

(3) Gajdács, M. The Continuing Threat of Methicillin-Resistant Staphylococcus aureus. *Antibiotics* **2019**, *8*, 52.

(4) Chojnacki, M.; Wucher, B.; Reed, J. N.; Tomaras, A.; Dunman, P. M.; Wozniak, R. A. F. Development of a Broad-Spectrum Antimicrobial Combination for the Treatment of Staphylococcus aureus and Pseudomonas aeruginosa Corneal Infections. *Antimicrob. Agents Chemother.* **2019**, *63*, e01929−e02018.

(5) Dawan, J.; Arunpoo, J. Assessment of β-Lactamase Inhibitor Potential of Medicinal Plant Extracts against Antibiotic-resistant Staphylococcus aureus. *Korean J. Plant Res.* **2020**, *33*, 578−585.

(6) Liu, W.-T.; Chen, E.-Z.; Yang, L.; Peng, C.; Wang, Q.; Xu, Z.; Chen, D.-Q. Emerging resistance mechanisms for 4 types of common anti-MRSA antibiotics in Staphylococcus aureus: A comprehensive review. *Microb. Pathog.* **2021**, *156*, 104915.

(7) Fisher, J. F.; Mobashery, S. β-Lactams against the Fortress of the Gram-Positive Staphylococcus aureus Bacterium. *Chem. Rev.* **2021**, *121*, 3412−3463.

(8) Sharmin, S.; Rahaman, M. M.; Sarkar, C.; Atolani, O.; Islam, M. T.; Adeyemi, O. S. Nanoparticles as Antimicrobial and Antiviral Agents: A Literature-Based Perspective. *Heliyon* **2021**, *7*, No. e06456.

(9) Imani, S. M.; Ladouceur, L.; Marshall, T.; Maclachlan, R.; Soleymani, L.; Didar, T. F. Antimicrobial Nanomaterials and Coatings: Current Mechanisms and Future Perspectives to Control the Spread of Viruses Including SARS-CoV-2. *ACS Nano* **2020**, *14*, 12341−12369.

(10) Wang, L.; Hu, C.; Shao, L. The antimicrobial activity of nanoparticles: present situation and prospects for the future. *Nanomedicine* **2017**, *12*, 1227−1249.

(11) Naveed, M.; Batool, H.; Rehman, S. u.; Javed, A.; Makhdoom, S. I.; Aziz, T.; Mohamed, A. A.; Sameeh, M. Y.; Alruways, M. W.; Dablool, A. S.; Almalki, A. A.; Alamri, A. S.; Alhomrani, M. Characterization and Evaluation of the Antioxidant, Antidiabetic, Anti-Inflammatory, and Cytotoxic Activities of Silver Nanoparticles Synthesized Using Brachychiton populneus Leaf Extract. *Processes* **2022**, *10*, 1521.

(12) Naveed, M.; Bukhari, B.; Aziz, T.; Zaib, S.; Mansoor, M. A.; Khan, A. A.; Shahzad, M.; Dablool, A. S.; Alruways, M. W.; Almalki, A. A.; Alamri, A. S.; Alhomrani, M. Green Synthesis of Silver Nanoparticles Using the Plant Extract of Acer oblongifolium and Study of Its Antibacterial and Antiproliferative Activity via Mathematical Approaches. *Molecules* **2022**, *27*, 4226.

(13) Saleem, A.; Afzal, M.; Naveed, M.; Makhdoom, S. I.; Mazhar, M.; Aziz, T.; Khan, A. A.; Kamal, Z.; Shahzad, M.; Alharbi, M.; Alshammari, A. HPLC, FTIR and GC-MS Analyses of Thymus vulgaris Phytochemicals Executing In Vitro and In Vivo Biological Activities and Effects on COX-1, COX-2 and Gastric Cancer Genes Computationally. *Molecules* **2022**, *27*, 8512.

(14) Naveed, M.; Makhdoom, S. I.; Rehman, S. u.; Aziz, T.; Bashir, F.; Ali, U.; Alharbi, M.; Alshammari, A.; Alasmari, A. F. Biosynthesis and Mathematical Interpretation of Zero-Valent Iron NPs Using Nigella sativa Seed Tincture for Indemnification of Carcinogenic Metals Present in Industrial Effluents. *Molecules* **2023**, *28*, 3299.

(15) Hayat, P.; Khan, I.; Rehman, A.; Jamil, T.; Hayat, A.; Rehman, M. U.; Ullah, N.; Sarwar, A.; Alharbi, A. A.; Dablool, A. S.; Daudzai, Z.; Alamri, A. S.; Alhomrani, M.; Aziz, T. Myogenesis and Analysis of Antimicrobial Potential of Silver Nanoparticles (AgNPs) against Pathogenic Bacteria. *Molecules* **2023**, *28*, 637.

(16) Xiong, Y.; Ng, K.; Zhang, P.; Warner, R. D.; Shen, S.; Tang, H.-Y.; Liang, Z.; Fang, Z. In Vitro α-Glucosidase and α-Amylase Inhibitory Activities of Free and Bound Phenolic Extracts from the Bran and Kernel Fractions of Five Sorghum Grain Genotypes. *Foods* **2020**, *9*, 1301.

(17) Ou, C.; Shang, D.; Yang, J.; Chen, B.; Chang, J.; Jin, F.; Shi, C. Prevalence of multidrug-resistant Staphylococcus aureus isolates with strong biofilm formation ability among animal-based food in Shanghai. *Food Control* **2020**, *112*, 107106.

(18) Gatadi, S.; Madhavi, Y. V.; Chopra, S.; Nanduri, S. Promising antibacterial agents against multidrug resistant Staphylococcus aureus. *Bioorg. Chem.* **2019**, *92*, 103252.

(19) Ge, B.; Mukherjee, S.; Hsu, C.-H.; Davis, J. A.; Tran, T. T. T.; Yang, Q.; Abbott, J. W.; Ayers, S. L.; Young, S. R.; Crarey, E. T.; Womack, N. A.; Zhao, S.; McDermott, P. F. MRSA and multidrug-resistant Staphylococcus aureus in U.S. retail meats, 2010−2011. *Food Microbiol.* **2017**, *62*, 289−297.

(20) Mokarroma, S.; Shammi, T. Determination of In vitro antimicrobial activity of homeopathy medicines. *Stamford J. Microbiol.* **2019**, *8*, 7−9.

(21) Carcione, D.; Siracusa, C.; Sulejmani, A.; Leoni, V.; Intra, J. J. A. Old and New Beta-Lactamase Inhibitors: Molecular Structure, Mechanism of Action, and Clinical Use. *Antibiotics* **2021**, *10*, 995.